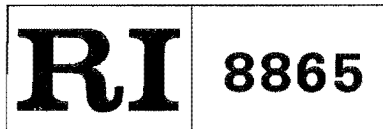


RI 8865



Bureau of Mines Report of Investigations/1984

# The Theory of Flammability Limits

Flow Gradient Effects and Flame Stretch

By Martin Hertzberg



UNITED STATES DEPARTMENT OF THE INTERIOR

**Report of Investigations 8865**

# **The Theory of Flammability Limits**

**Flow Gradient Effects and Flame Stretch**

**By Martin Hertzberg**



**UNITED STATES DEPARTMENT OF THE INTERIOR**

**William P. Clark, Secretary**

**BUREAU OF MINES**

**Robert C. Horton, Director**

Library of Congress Cataloging in Publication Data:

**Hertzberg, Martin**

The theory of flammability limits: flow gradient effects and flame stretch.

(Report of investigations ; 8865)

Bibliography: p. 32-34.

Supt. of Docs. no.: I 28.23:8865.

I. Flame. 2. Combustion, Theory of. I. Title. II. Series: Report of investigations (United States. Bureau of Mines) ; 8865. III. Title. Flammability limits.

TN23.U43 [QD5 16] 622s [621.402'3] 83-600372

## CONTENTS

	<u>Page</u>
Abstract.....	1
Introduction.....	2
Flame stretch limit burning velocity, $(S_u)_e$ .....	3
Equivalence in terms of Karlovitz number and Markstein hypothesis.....	7
Comparison of theoretical limit velocity gradients for flame stretch extinction with measured boundary velocity gradients at blowoff.....	8
Bunsen flame.....	9
Inverted flame.....	14
Counterflow flame.....	18
Normal limit for upward flame propagation: flame stretch under natural convection.....	22
Maximum buoyant rise velocity for spherical propagation.....	22
Recent estimates and observations of buoyancy-induced limits.....	24
Flow-field solutions for spherical propagation in buoyancy-induced flows: flame stretch limit for upward propagation.....	26
References.....	32
Appendix.--Symbols and nomenclature.....	35

## ILLUSTRATIONS

1. Divergence losses in spherical flame propagation from a flame front of finite thickness.....	4
2. Stretching of a flame front surface by propagation into a velocity gradient.....	6
3. Flat flame and Bunsen flame burner velocity profiles: flame zone stretch of the Bunsen flame.....	9
4. Blowoff limits for premixed, methane-air flames: comparison of data for Bunsen burners in an ambient air environment with theory.....	11
5. Blowoff limits for premixed, methane-air flames: comparison of data for Bunsen burners in an $N_2$ environment with theory.....	13
6. Blowoff limits for inverted, premixed methane-air flames: comparison of data for slotted burners of varying plate thickness with theory.....	15
7. Dilution of the velocity gradient by flow expansion beyond the corner of the interior boundary or holding edge of an inverted flame.....	16
8. Extrapolation of calculated boundary velocity gradients to zero plate thickness for inverted methane-air flames.....	17
9. Blowoff limits of premixed, methane-air flames: final comparison of corrected data with theory.....	18
10. Domains of stability and extinction for premixed normal (rim flames) and for premixed stretched (flat flames) in a stagnation-plate flow configuration.....	20
11. Blowoff (extinction) limits for premixed propane-air flames in counterflow and stagnation plate flow configurations compared with theory and with normal blowoff limits for Bunsen flames in air.....	21
12. Idealized motions and approximate real motions during the buoyant rise of an outward-propagating, spherical, flame kernel under the simultaneous influence of the combustion force expansion and the buoyancy force couple	23
13. Buoyancy-induced, flow-field vectors of the unburned gas around a rising, spherical flame kernel from classical Stokes flow solutions past a sphere	27

## ILLUSTRATIONS--Continued

Page

14. Simple vector sums of combustion force expansion flow field and the buoyancy-induced Stokes flow field, assumed to be operating independently in steady state..... 29
15. Position of the stagnation point above the upward hemisphere of a rising and expanding flame kernel as a function of the ratio of buoyant velocity to burning velocity..... 31

## UNIT OF MEASURE ABBREVIATIONS USED IN THIS REPORT

cm	centimeter	mm	millimeter
cm/sec	centimeter per second	m/sec	meter per second
cm/sec <sup>2</sup>	centimeter per square second	pct	percent
cm <sup>2</sup> /sec	square centimeter per second	sec	second
m	meter	vol-pct	volume-percent

# THE THEORY OF FLAMMABILITY LIMITS

## Flow Gradient Effects and Flame Stretch

By Martin Hertzberg<sup>1</sup>

---

### ABSTRACT

In this Bureau of Mines study, an equation is derived for the limit burning velocity for divergent, spherical propagation from an ignition kernel of radius,  $r$ :  $(S_u)_e = \frac{2\alpha}{r} \frac{\rho_u}{\rho_b}$ . For flame propagation into a preexisting, stretching velocity gradient of magnitude  $dv/dx$ , the limit velocity is  $(S_u)_e = (\alpha dv/dx)^{1/2}$ . These formulations are shown to be equivalent to the fluid dynamic concepts of Damkohler, Karlovitz, and Markstein. Existing data for the blowoff limits of flames are shown to give excellent agreement with those concepts provided that proper account is taken of two dilution effects: composition dilution caused by entrainment and velocity gradient dilution caused by flow expansion.

Approximate flow-field solutions are also derived for the unburned gas motion above an upward propagating, spherical flame kernel in buoyancy-induced flows. It is shown that the upward hemisphere propagates toward a stagnation plane in a counterflow configuration involving the balance between the combustion force, which accelerates the cold gas upward, and the buoyancy force that accelerates the cold gas downward. The position of the stagnation plane above the upward propagating hemisphere is related to the ratio of the buoyant velocity,  $v_b$ , to the burning velocity,  $S_u$ . Extinction of the upward propagating wave occurs by flame stretch in that counterflow configuration when  $\eta = v_b/S_u$  begins to exceed the expansion ratio,  $\rho_u/\rho_b$ , and the wave is blown off by its own buoyancy-induced flow field.

---

<sup>1</sup>Supervisory research chemist, Pittsburgh Research Center, Bureau of Mines, Pittsburgh, PA

## INTRODUCTION

In earlier Bureau of Mines reports (1-3),<sup>2</sup> the concept of limit burning velocities was developed and used to formulate a quantitative theory of flammability limits. The concept was developed by first considering the normal (laminar) mode of flame propagation in an exothermic gas mixture. Such normal propagation is characterized by a convective flow "eigenvalue" solution to the time-dependent conservation equations. That eigenvalue, or ideal burning velocity  $(S_u)_{ideal}$ , is, in principle, a measurable parameter whose value in an adiabatic system is a unique function of its initial thermodynamic state. Generally, measured  $S_u$  values are in good agreement with exact solutions to the conservation equations that are based on reasonable estimates of transport coefficients, plausible kinetic mechanisms for the combustion reactions, and reasonable values for the appropriate rate coefficients (4).

That agreement between theory and experiment is good so long as the reactant compositions are well within the empirically measured domain of flammability. However, those same conservation equations in a laminar, adiabatic system generate finite  $(S_u)_{ideal}$  solutions for compositions well outside of the flammability range. No matter how small the exothermicity, so long as it is finite and the system is adiabatic, solutions are generated for the normal burning velocity and also for the flame temperature. Yet, the measured burning velocities and the observed flame temperature drop almost discontinuously to zero at the limits of flammability, and remain at zero for all compositions beyond those limits. Why? What is the physical cause of the existence of those discontinuities?

Although there is nothing in the laminar, adiabatic solutions that can generate such flammability limit discontinuities, it has long been known that for nonadiabatic systems finite limit discontinuities will appear. These were the subject of earlier reports (1-3). The consideration of such nonadiabatic systems inevitably involves multidimensional solutions to the conservation equations. The various nonadiabatic processes that compete with the flame propagation process and thus dissipate power from the combustion wave, were enumerated as (a) free, buoyant convection, (b) conductive-convective wall losses, (c) radiative losses, (d) selective diffusional demixing, and (e) flame stretch or flow-gradient losses. It was shown that the very existence of limits of flammability at finite fuel concentrations was caused by the competition between those loss processes and the normal flame propagation process. The concept of limit burning velocities was developed by considering the balance between the rate of thermal energy generation in an adiabatic or ideal propagating flame front and the rate of energy loss from those various competing processes. Those competing processes dissipate power from the wave to the surroundings. A quantitative measure of the magnitude or influence of a dissipative process was its limit burning velocity: the larger the limit velocity the more significant the process. Propagation is thus possible only if the ideal burning velocity exceeds the limit velocity.

The first in this series of reports (1) considered process a, natural convection. The second in this series (2) considered process b, conductive-convective wall losses. The third (3) considered process c, radiative losses, and also process d, selective diffusional demixing. This report, which is the fourth of the series, considers process e, flow gradient effects or flame stretch.

---

<sup>2</sup>Underlined numbers in parentheses refer to items in the list of references preceding the appendix.

While each process has been considered in sequence, there are many cases where they do not act independently but where they are coupled in complicated ways. For example, it has already been necessary to introduce the concept of a flame stretch limit velocity,  $(S_u)_e$ , in the consideration of processes a and d (1, 3). Although process e is a loss process, it differs significantly from the other nonadiabatic loss processes. In the other loss processes, b and c, the surroundings to which heat was lost were either inert walls or external regions far removed from the flame front. For process e, the quenching "surroundings" are internal; that is they are normally a part of the reacting system. For process e, it is the unburned exothermic mixture immediately adjacent to the flame front, that serves as the cold, quenching medium. Under nonstretch or laminar conditions, that region is normally activated and propagates flame, but under stretch conditions it quenches the flame. It is a kind of internal nonadiabaticity caused either by the curvature of a flame front; or by the velocity gradients in the unburned, cold surroundings from which that front is being generated and into which it is propagating.

#### FLAME STRETCH LIMIT BURNING VELOCITY, $(S_u)_e$

An ideal, laminar combustion wave of infinite extent propagates through a flammable mixture at the velocity  $(S_u)_{ideal}$ . That velocity reflects a complex mechanism of activation of cold, unburned mixture by the back diffusion of heat and free radicals from the hot, burned mixture; and the subsequent exothermic chemical reactions that regenerate them and sustain the laminar propagation process. For a laminar wave geometry traversing into a gas which is quiescent, or in a uniform state of rectilinear motion, those activation flow densities are invariant and steady-state propagation results. There is no divergence or convergence in those diffusional activation flows and hence there is no loss or gain in the enthalpy feedback across the wave front as it propagates. However, in the presence of curvature, the activation flow densities are not invariant and there are losses or gains in the enthalpy feedback flux as the wave propagates.

Consider the problem in general terms as follows. A burned gas volume that is bounded by a flame front, whose surface area is  $A_s$ , is expanding into a cold, unburned region. If  $\Delta x$  is the flame front thickness, then the instantaneous flame front volume within which active propagation is occurring is given by  $V_\delta = A_s \Delta x$ . Let the rate of expansion of that flame front volume be given by  $dV_\delta/dt$ . In the presence of flame propagation, the zone between the burned gas fireball and the unburned mixture is the active flame front whose thickness is  $\Delta x = \alpha/S_u$ . The combustion power density across that flame front is  $S_u c \rho (T_b - T_u)$  and therefore the volumetric flame front heating rate in that zone is

$$\dot{q}(\text{heating}) = S_u c \rho (T_b - T_u) / \Delta x = S_u^2 c \rho (T_b - T_u) / \alpha. \quad (1)$$

Now in the absence of flame propagation, the expansion of a hot fireball surface at temperature  $T_b$  into cold surrounding at temperature  $T_u$  would result in a volumetric cooling rate within that same volume of

$$\dot{q}(\text{cooling}) = c \rho (T_b - T_u) \frac{1}{V_\delta} \frac{dV_\delta}{dt}, \quad (2)$$

where  $c$  is the heat capacity of the mixing zone and  $\rho$  is the density. What was considered as the flame front volume,  $V_\delta$ , in the presence of flame propagation, may alternatively, in the absence of propagation, be considered as the mixing or cooling volume between hot, burned gas and cold, unburned gas. Quenching of flame propagation occurs when the flame's normal volumetric heating rate in the presence of propagation would be just balanced by the volumetric cooling rate resulting from

expansion of that volume into cold surroundings in the absence of propagation; that is, when  $\dot{q}(\text{heating}) = \dot{q}(\text{cooling})$ . For spherical propagation

$$\frac{1}{V_\delta} \frac{dV_\delta}{dt} = \frac{1}{V_\delta} \frac{dV_\delta}{dr} \frac{dr}{dt} = \frac{1}{V_\delta} \frac{dV_\delta}{dr} S_u \rho_u / \rho_b, \quad (3)$$

where  $r$  is the radial distance of the flame front from the point of ignition. Setting equation 1 equal to equation 2, substituting equation 3 into the resultant equation, and solving for the burning velocity at that quenching limit gives

$$(S_u)_e = \alpha \frac{\rho_u}{\rho_b} \frac{1}{V_\delta} \frac{dV_\delta}{dr}. \quad (4)$$

The quantity  $\frac{1}{V_\delta} \frac{dV_\delta}{dr}$  is the volumetric divergence of the flame in the propagation direction. For the planar case there is no divergence; that is,  $\frac{dV_\delta}{dr} = 0$  and the flame front volume remains constant as propagation proceeds. In that case there are no flame stretch losses and  $(S_u)_e = 0$ .

For spherical propagation, however, there are finite divergence losses as depicted in figure 1. For the spherical case,  $V_\delta = 4\pi r^2 \Delta x$  and hence  $\frac{1}{V_\delta} \frac{dV_\delta}{dr} = \frac{2}{r}$ .

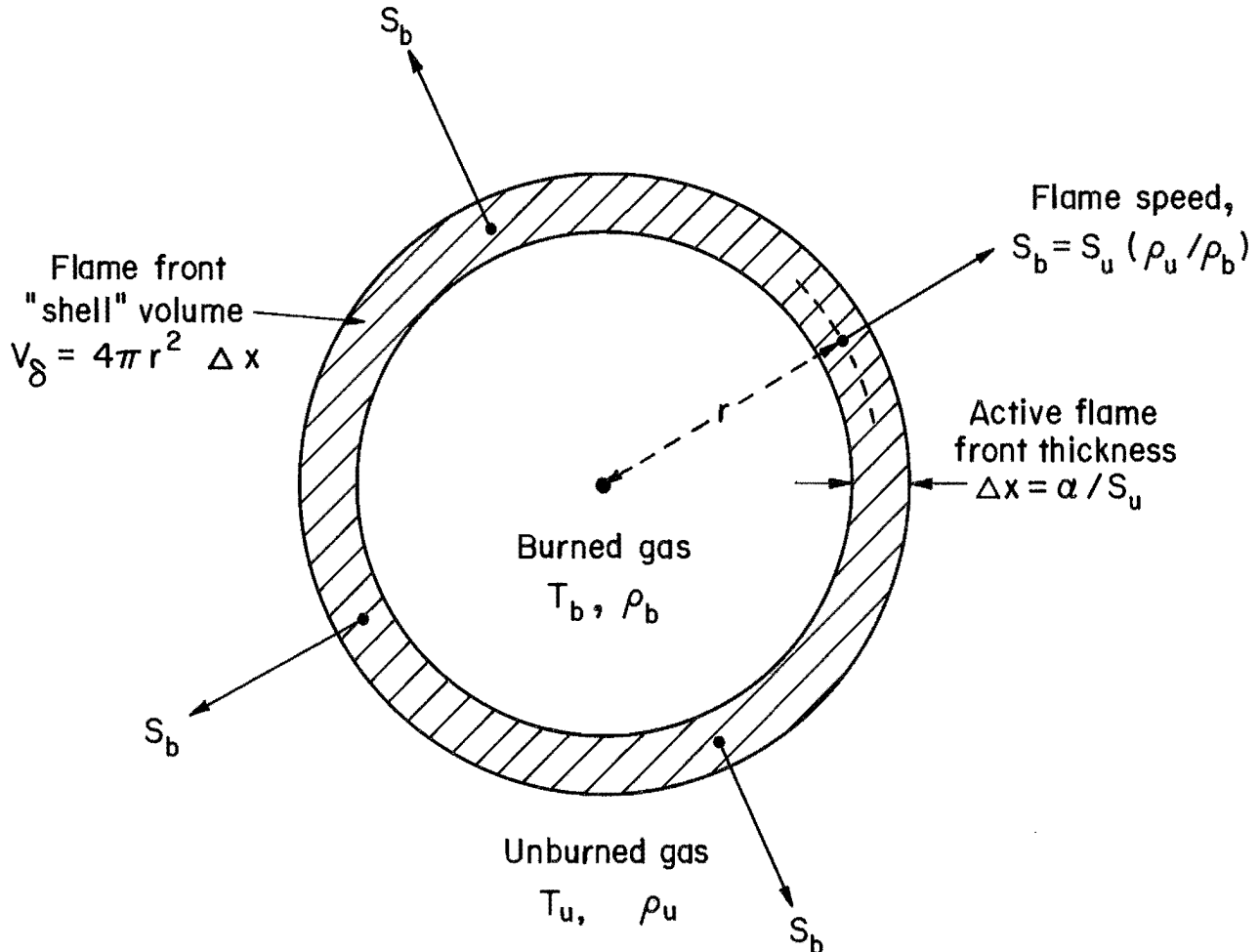


FIGURE 1. • Divergence losses in spherical flame propagation from a flame front of finite thickness.

Substituting into equation 4 gives

$$(S_u)_e = \frac{2\alpha}{r} \frac{\rho_u}{\rho_b}. \quad (5)$$

It is no coincidence that the functional form of this limit velocity for flame stretch quenching (process e) is identical to that derived for wall loss quenching (process b) (2). Wall losses are characterized by a tubular quenching diameter,  $d_q$ , whose value was predictable in terms of a special kind of Peclet number,  $Pe = S_u d_q / \alpha$ . Critical Peclet constants for wall quenching were in the range  $Pe \approx 20$  to 25. For stretch quenching, setting  $r = d_q/2$  for the minimum radius that can freely propagate, and substituting into equation 5, gives  $Pe$  (stretch) =  $4 \rho_u / \rho_b$ . A typical near-limit density ratio is  $\rho_u / \rho_b \approx 5$ , so that  $Pe$  (stretch)  $\approx 20$ . Thus the same Peclet constant is obtained for flame stretch quenching as was obtained for wall loss quenching. Clearly analogous loss processes are involved. In the latter case (2), quenching occurs because of enthalpy losses in the two directions perpendicular to the propagation direction, to a quenched boundary layer in contact with a cold, tube wall. In the former case being considered here, quenching is caused by enthalpy divergence losses to cold gases that envelop the flame kernel from all three directions. In the latter case, heat losses in the two perpendicular directions are equivalent to an enthalpy divergence. In this former case of divergent propagation, the excess mass flux of cold gas that must be activated by the flame kernel serves, in effect, as a cold, quenching boundary.

In the case just considered (fig. 1), the expansion of the flame front volume is caused by the divergent configuration of the flame front: its initiation at a point, and the resultant spherical curvature that is reflected in the  $1/r$  dependence for the limit velocity in equation 5. There are other conditions, however, that can cause such expansions or divergent configurations. One has already been discussed in relation to cellular flame structures caused by selective diffusion (3). Such cellular flame structures appear spontaneously even if the wave is initially planar. Equation 5 has already been used in that case to develop an equation that properly predicted the diameters of such cellular structures. Another, more common process that causes such divergence involves the propagation of a flame front into a preexisting velocity gradient in the unburned gas. In such a case, the flame front is constrained to propagate with that cold gas velocity component superimposed on its normal or laminar velocity with respect to the unburned mixture.

When propagation into such a velocity gradient field occurs, flow continuity constraints cause a stretching of the flame front, an inevitable readjustment of the propagation directions, and a change in the shape of the flame front. The problem was clearly formulated by Karlovitz (5), and figure 2 is reproduced from that work. To quote the analysis:

"At point 1 the combustion wave enters the segment 1-2 with the small velocity component  $U_1 \cos \phi_1$ , parallel to the wave surface; at point 2 it leaves with the larger velocity component  $U_2 \cos \phi_2$ . Thus new flame surface is produced continually as the flame traverses the velocity gradient. As a consequence of this 'stretching' of the flame surface, the amount of heat flowing from the reaction zone of the flame into the unburned gas is distributed over increasing volumes of gas, which means that the burning velocity must decrease."

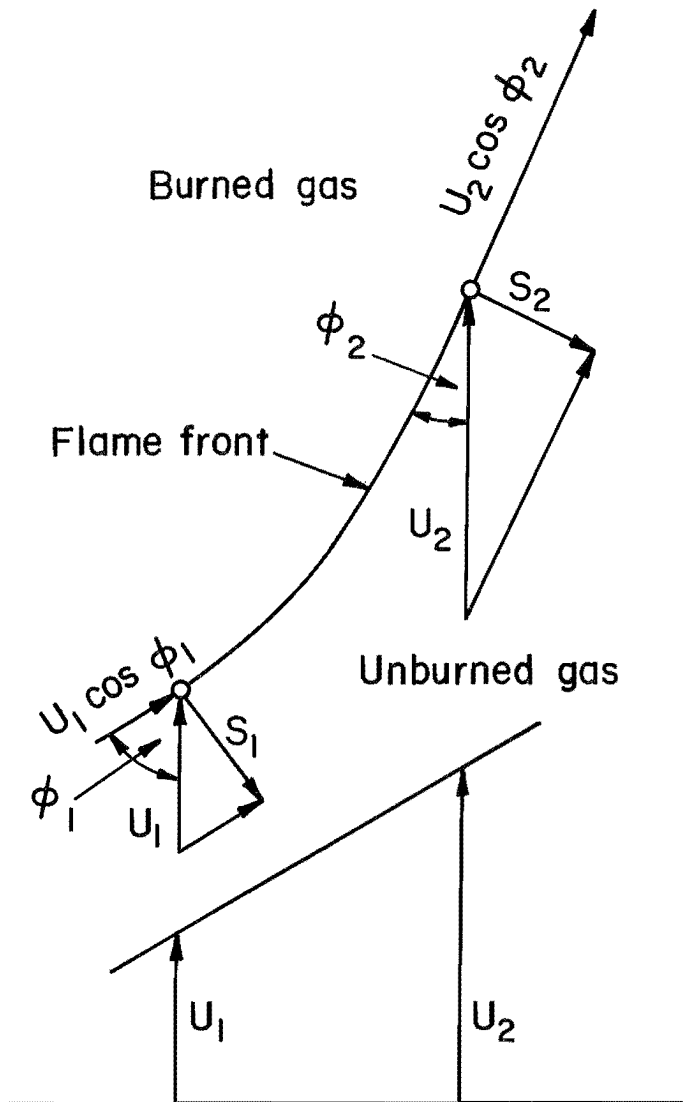


FIGURE 2. - Stretching of a flame front surface by propagation into a velocity gradient.

elements of the unburned mixture must be continuously accommodated during the characteristic reaction time,  $\tau_{pm}$ . The reciprocal of the velocity gradient,  $(dv/dx)^{-1}$ , is in effect a residence time,  $\tau_r$ , for these new volume elements passing into the flame front. If that residence time is too short they cannot be activated during the characteristic reaction time,  $\tau_{pm}$ , and they quench the flame. For the limit condition, one sets  $\tau_{pm} = \tau_r$  and obtains equation 7. The ratio  $\tau_r/\tau_{pm}$  is, in effect, the Damkohler number for the flame front propagating into a velocity gradient.

It should be recognized that the losses associated with the flame stretch process caused by such divergent propagation become enthalpy gains when the propagation becomes convergent, or the curvature is reversed so that it becomes concave to the unburned mixture.

One such example is the apex of the typical Bunsen burner flame. There the curvature is concave to the unburned mixture, rather than convex as in the spherically divergent flame depicted in figure 1. At the apex of the Bunsen flame, the back

For propagation into such a velocity gradient, the rate of expansion of the flame front volume (or surface) is, in effect, the component of the velocity gradient,  $dv/dx$ , that stretches it. Thus

$$\frac{1}{V_\delta} \frac{dV_\delta}{dt} = \frac{dv}{dx}. \quad (6)$$

Combining equations 1, 2, and 3 for this case gives

$$(S_u)_e = \left[ \alpha \frac{dv}{dx} \right]^{1/2}. \quad (7)$$

The preexisting velocity gradient that stretches the flame front forces it to "swallow" a greater mass flux of cold, unburned mixture than it would normally consume in ideal, laminar propagation.

In an equivalent derivation of equation 7, one notes that the normal or ideal flame zone thickness in the absence of convective gradients is  $\Delta x = \alpha/S_u$ . Since the flame propagates through that thickness at a velocity  $S_u$ , the characteristic time for the completion of the reactions associated with premixed flame propagation, is  $\tau_{pm} = \Delta x/S_u = \alpha/S_u^2$ .

In the presence of uniform translational motion, there is no stretch and every element of the flame front adjusts uniformly to the rectilinear motion. However, when a velocity gradient stretches the flame, larger volume

diffusional flows from the burned mixture are convergent and there is a large magnification or increase in the burning velocity (6). Another example would involve a turbulent system in which the turbulence is isotropic. In that case, for every region of space where the flame front is stretched by velocity gradients of one sign, there must exist complementary regions where the front is compressed by gradients of opposite sign.

As with other limit velocities previously derived,  $(S_u)_e$  may also be viewed as the magnitude of the burning velocity decrease that results from the presence of the competing process. For convergent propagation or compressed flame fronts, equations 4 and 7 would thus correspond to the resultant increases in burning velocity.

#### EQUIVALENCE IN TERMS OF KARLOVITZ NUMBER AND MARKSTEIN HYPOTHESIS

As indicated in figure 2, the problem of flame propagation in velocity gradients was formulated by Karlovitz (5). New flame surface is produced in the case shown at a rate proportional to the velocity gradient normal to the propagation direction. The flame is thus stretched and the burning velocity decreases proportionately. The concept was initially applied to the problem of turbulent flame propagation and to the "break off" of flames in a turbulent boundary layer. Lewis and von Elbe (6) went further by defining a dimensionless Karlovitz number,  $K$ , which was applied to a variety of quenching phenomena. For the first case of divergent propagation from a spherical ignition kernel, as indicated in figure 1, enthalpy flows from that kernel cannot activate the unburned mixture until they penetrate the finite distance of one flame zone thickness,  $\Delta x$ , into the cold gas surrounding it. Thus the area to be activated in divergent propagation is larger than the source area by the factor  $1 + 2(\Delta x/r)(\rho_u/\rho_b)$ . The area increase or "stretch factor,"  $2(\Delta x/r)(\rho_u/\rho_b)$ , was defined as the Karlovitz number. Setting  $\Delta x = \alpha/S_u$  gives the identical functional form to that of equation 5. Thus the definition of the limit burning velocity  $(S_u)_e$  given in equation 5 is identical to the assertion that flame stretch quenching occurs in divergent propagation if  $K > 1$ .

Lewis and von Elbe also applied the concept to the problem of ignition from a minimum critical flame diameter. A minimum ignition energy is necessary in order to activate a source volume or ignition kernel that is initially large enough to overcome the divergence losses. Lewis identified  $d = 2r_q$  with experimental quenching distances determined by separating spark electrodes to the point of the lowest value of the minimum ignition energy. The values of  $K = (2\alpha/r_q S_u)(\rho_u/\rho_b)$  so obtained were all near unity even though  $S_u$  values for the mixtures studied varied from as low as 12 cm/sec to as high as 400 cm/sec; and  $\rho_u/\rho_b$  values varied from as low as 5.5 to as high as 14.5.

For the other case of flame propagation in velocity gradients, Lewis and von Elbe defined the Karlovitz number as the fractional change in flow velocity, caused by the preexisting velocity gradient, across the finite thickness of flame front. Thus  $K = \Delta v/v = (dv/dx)\Delta x/v$ . If one chooses a coordinate system that is moving with the wave in steady state at the average velocity in that gradient, one has  $S_u \approx v$ . Setting  $\Delta x = \alpha/S_u$  gives equation 7 for a Karlovitz number of unity.

The Markstein hypothesis (7) was a proposed dependence for the burning velocity on flame front curvature of the form  $S_u = (S_u)_{ideal} [1 + L/r]$ , where  $r$  is the radius of curvature of the flame front and  $L$  is a characteristic length related to the flame zone thickness,  $\Delta x$ . The problem under consideration by Markstein was the general problem of the stability of flame fronts and their response to perturbations. Such perturbations could involve either changes in flame front shape (curvature) or in the

structure of the flow field, and it was necessary to know how the instantaneous or local burning velocity,  $S_u$ , would respond to such perturbations in order to proceed with the stability analysis. Markstein proposed the above relationship on the basis of the available experimental evidence. As given, the formula associates an increase in burning velocity with strongly curved flame fronts. As indicated earlier, such is the case for the apex or tip of a Bunsen burner where the curvature is concave toward the unburned mixture entering the flame front. In that case there is a convergence of diffusional flows from the burned products into the unburned mixture. There is, therefore, a net gain in enthalpy flux, and  $S_u$  increases.

For the case being considered in figure 1, the curvature is convex to the unburned medium to be activated. In that case, the activating fluxes are divergent and there is a decrease in  $S_u$ , so that the Markstein relationship becomes  $S_u = (S_u)_{ideal} [1-L/r]$ . Since  $L$  was a characteristic length related to the flame zone thickness  $\Delta x$ , one sets  $L = k \Delta x = k\alpha/(S_u)_{ideal}$ . Substituting that value into the Markstein relation gives  $[(S_u)_{ideal} - S_u] = k\alpha/r$ , where  $k$  is a constant of proportionality. As indicated earlier, the limit burning velocity  $(S_u)_e$  in equation 5 may also be viewed as the magnitude of the burning velocity decrease that results from the presence of the competing process  $e$ , and thus  $(S_u)_e = [(S_u)_{ideal} - S_u]$ . Substituting the latter equation into the Markstein relationship gives  $(S_u)_e = k\alpha/r$ , which becomes identical with equation 5 if it is assumed that  $k = 2 \rho_u/\rho_b$ . Thus the Markstein hypothesis is equivalent to equation 5 provided that the characteristic length is taken as  $L = 2 \rho_u/\rho_b \Delta x$ . Markstein hypothesized that  $L$  was "assumed to be of the order of the thickness of the flame zone." The derivation of equation 5 and the available experimental evidence suggest that it is twice the size of the characteristic flame zone thickness,  $\Delta x$ , multiplied by the expansion ratio,  $\rho_u/\rho_b$ .

#### COMPARISON OF THEORETICAL LIMIT VELOCITY GRADIENTS FOR FLAME STRETCH EXTINCTION WITH MEASURED BOUNDARY VELOCITY GRADIENTS AT BLOWOFF

For any given quenching process, the magnitude of its limit velocity is a measure of its significance in determining the limit of flammability. The larger the limit velocity,  $(S_u)_{a,b,c}$ , or  $e$ , relative to  $(S_u)_{ideal}$ , the more significant the process. For flame stretch, the limit velocity is  $(S_u)_e$ , and the larger it is relative to  $(S_u)_{ideal}$  the more significant is flame stretch in determining the limit. If, on the other hand, the sum of all relevant limit velocities is much smaller than the normal or ideal burning velocity, then flame propagation will proceed in the normal way. Such is the case for a typical, stoichiometric hydrocarbon-air mixture in a large-diameter tube or container in the earth's gravitational field. For stoichiometric, saturated hydrocarbons in air  $(S_u)_{ideal} \approx 45$  cm/sec and that value is much larger than the applicable limit velocity for buoyant quenching,  $(S_u)_a$ , which is in the range of 3 to 6 cm/sec. The stoichiometric mixture propagates "normally" with no hint or evidence of a limit discontinuity. If, however, the stoichiometric mixture is diluted with excess air, excess fuel, or excess inert gas, then  $(S_u)_{ideal}$  diminishes and a limit condition is approached. Alternatively, if the quenching process is magnified in some way--such as by increasing gravity or by wall heat losses--then the limit velocities are increased and a limit is approached even for a stoichiometric mixture. The limit condition is reached when the limit velocity (or the applicable sum of limit velocities) is just equal to the ideal burning velocity. Thus, according to equation 7 any fuel-air mixture can be quenched by a stretching velocity gradient whose magnitude exceeds the value

$$\left(\frac{dv}{dx}\right)_{limit} = (S_u)_{ideal}^2 / \alpha. \quad (8)$$

### Bunsen Flame

The case of flame stretch extinction that has been most extensively studied, as such, involves the Bunsen burner flame at high gas-flow velocities. At high flow velocities of the premixed fuel-air mixture, a "blowoff" limit is reached at which the flame is extinguished by the velocity gradient at the boundary of the inlet gas flow stream. Let us consider that case in detail and compare the available data with the predictions of equation 8.

For the laminar flow of the unburned fuel-air mixture in a cylindrical, Bunsen-burner tube, the radial velocity distribution is given by

$$v(r) = \frac{1}{4\eta} \frac{dp}{dz} (r_0^2 - r^2), \quad (9)$$

where  $\eta$  is the gas viscosity,  $dp/dz$  is the axial pressure gradient along the tube,  $r$  is the radial distance from the tube axis, and  $r_0$  is the tube's inner radius. This velocity distribution is the classical parabolic Poiseuille velocity profile for laminar flow in a cylindrical tube.

Some burner velocity profiles are depicted in figure 3. The simpler case of a flat-flame burner is depicted in figure 3A. It is contrasted with the Bunsen burner, which is characterized by the parabolic velocity profile sketched in figure 3B.

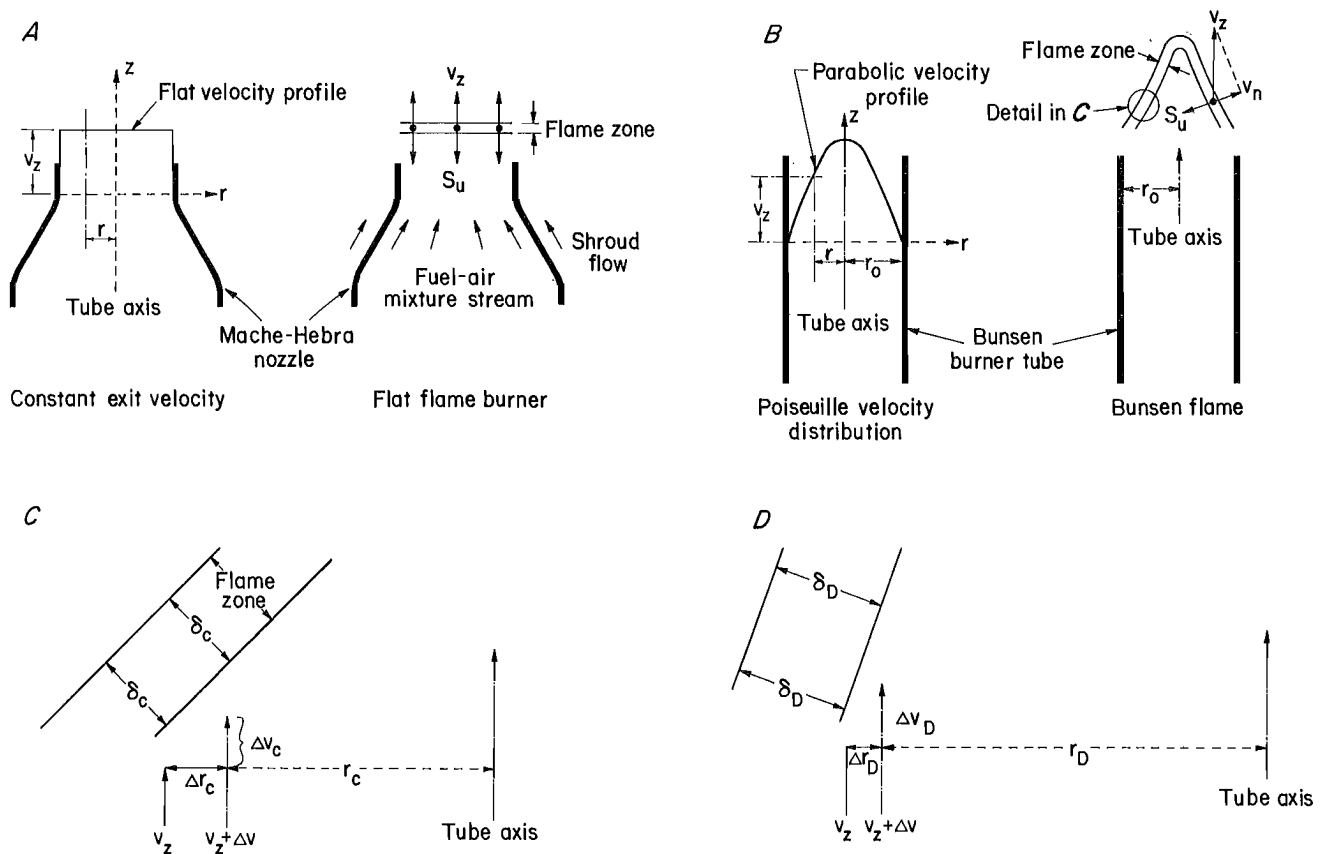


FIGURE 3. - Flat flame (A) and Bunsen flame (B) burner velocity profiles: flame zone stretch (C-D) of the Bunsen flame.

In figure 3A, one starts with a flat velocity profile in which there is no velocity gradient at the flame front. Such a flat profile can be obtained with either a Mache-Hebra nozzle (8-9) or with flow straighteners within the tube. To avoid flow gradients at the boundaries of the flat profile, the flammable mixture issuing from the burner, in figure 3A, can be surrounded by a shroud flow of inert gas. For the flat profile case, figure 3A, a steady state is obtained everywhere along the flame front when the constant exit flow velocity,  $v$ , matches the burning velocity,  $S_u$ . If the gas flow is increased and made larger than  $S_u$ , then the flame front moves upward, away from the burner surface. If the flow it is decreased, the front moves downward into the burner surface, and "flashes back" if the tube is open.

For the Bunsen burner flame depicted in figure 3B, there is a radial velocity profile in the tube given by equation 9. The velocity gradient is not zero except at the flame apex or in the center of the flow stream. The gradient is quite significant, especially near the tube wall where it is a maximum in the absence of any shroud flow. The quadratic velocity profile generates the curved flame shape that is approximately conical as depicted in figure 3B. There is now a complex balance of propagation directions that must match the flow profile of the incoming cold gas. The characteristic Bunsen shape is determined by the requirement that the burning velocity vector, which is always perpendicular to the flame front, must match the cold gas velocity component normal to the front,  $v_n$ . In steady state, the flame shape adjusts so that the condition  $S_u = -v_n$  is satisfied everywhere along the flame front. However, the Bunsen flame in figure 3B is now a stretched flame, especially at the flow streamlines just above the boundary near  $r = r_0$ . Not only is the velocity gradient a maximum in the boundary flow, but the flame curvature is also divergent there. Although the flame is also distorted by the velocity gradient along the flow axis near the flame apex, the gradient is minimal there and the flame curvature is convergent from the burned gas. For the same volumetric flow through the burners depicted in figures 3A and 3B, the Bunsen flame has a larger flame surface area than the flat flame. In figure 3A there is no flow gradient across the front thickness,  $\Delta x = \delta$ , whereas in figure 3B the propagation directions have been altered to accommodate the flow profile and there is a flow gradient across the front thickness. Thus the flame in figure 3B is a stretched flame, especially near the boundary above  $r = r_0$ , where the velocity gradient is a maximum across the finite thickness,  $\delta$ , of flame front. That stretched condition is depicted in detail in figure 3C. The flame zone has adjusted to account for the preexisting velocity increase,  $\Delta v_c$ , across its finite flame thickness,  $\delta_c$ . However, that increase in flame surface has stretched the flame, causing a reduction in the burning velocity, which causes the flame front to widen to a larger value,  $\delta_D$ , which is depicted in figure 3D. The lower  $S_u$  value now requires a lower  $v_n$  component, which steepens the flame front. Although the flame front is now wider, this can be compensated for by the fact that the component of flame thickness in the  $r$  direction is now smaller. Since  $\Delta v = (dv/dr) \Delta r$ , the reduction of  $\Delta r$  would tend to reduce  $\Delta v$ . However, note that the steepening of the front has also thrown that segment of the front outward from  $r_c$  to  $r_D$ , where the gradient is now steeper. Differentiating equation 9 with respect to  $r$  gives  $dv(r)/dr = -(1/2\eta)(dp/dx)r$ . The gradient thus increases as the front steepens and comes closer to the boundary of the flow at  $r = r_0$ . As shown in figure 3D, the increase in  $dv/dr$  is assumed to be larger than the decrease in  $\Delta r$ , so that  $\Delta v_D$  is shown to be larger than  $\Delta v_c$ . An exact solution to this problem is beyond the scope of these considerations and would require a detailed evaluation of expansion and entrainment effects beyond the burner exit, which tends to reduce the gradients and alter the gas composition by dilution with the entrained gases. Suffice to say that at some point, as the total flow through the burner is increased, the value of  $\Delta v$  across the widening flame front increases until it becomes comparable in magnitude to the initial average velocity,  $\bar{v}$ . At that point it is no longer possible for the flame front to

adjust to the gradient. It can no longer accommodate the increased cold gas flow in the residence time available for reaction, and the flame extinguishes; that is, it "blows off."

From the derivative of equation 9 with respect to  $r$  indicated above, the radial velocity gradient,  $dv(r)/dr$ , has its maximum value at  $r = r_0$ . That maximum velocity gradient occurs at the tube boundary and is thus referred to as the boundary velocity gradient,  $g_b$ . As the blowoff condition is approached and the flame front steepens, the propagation direction approaches the horizontal, and nearly the entire boundary velocity gradient appears across the flame front thickness,  $\delta$ . In that limit, researchers have generally made the assumption that

$$g_b = \left( \frac{dv(r)}{dr} \right)_{\text{at } r = r_0} = \frac{1}{2\eta} \frac{dp}{dz} r_0 = \left( \frac{dv}{dx} \right)_{\text{limit}}$$

The system that has been studied most extensively is methane in air. The data for the blowoff limits of premixed methane burner flames are shown in figure 4. The data by Grumer (10-11) are compared with the theoretical predictions of equation 8. The theoretical predictions are based upon the best available data for  $(S_u)_{\text{ideal}}$  taken from the measurements of Gunter (9), but adjusted slightly on the basis of the recent analysis and summary by Warnatz (4). The effective diffusivity of the flame zone is taken as  $\alpha = 0.55 \text{ cm}^2/\text{sec}$ , a value that has been used consistently in all previous

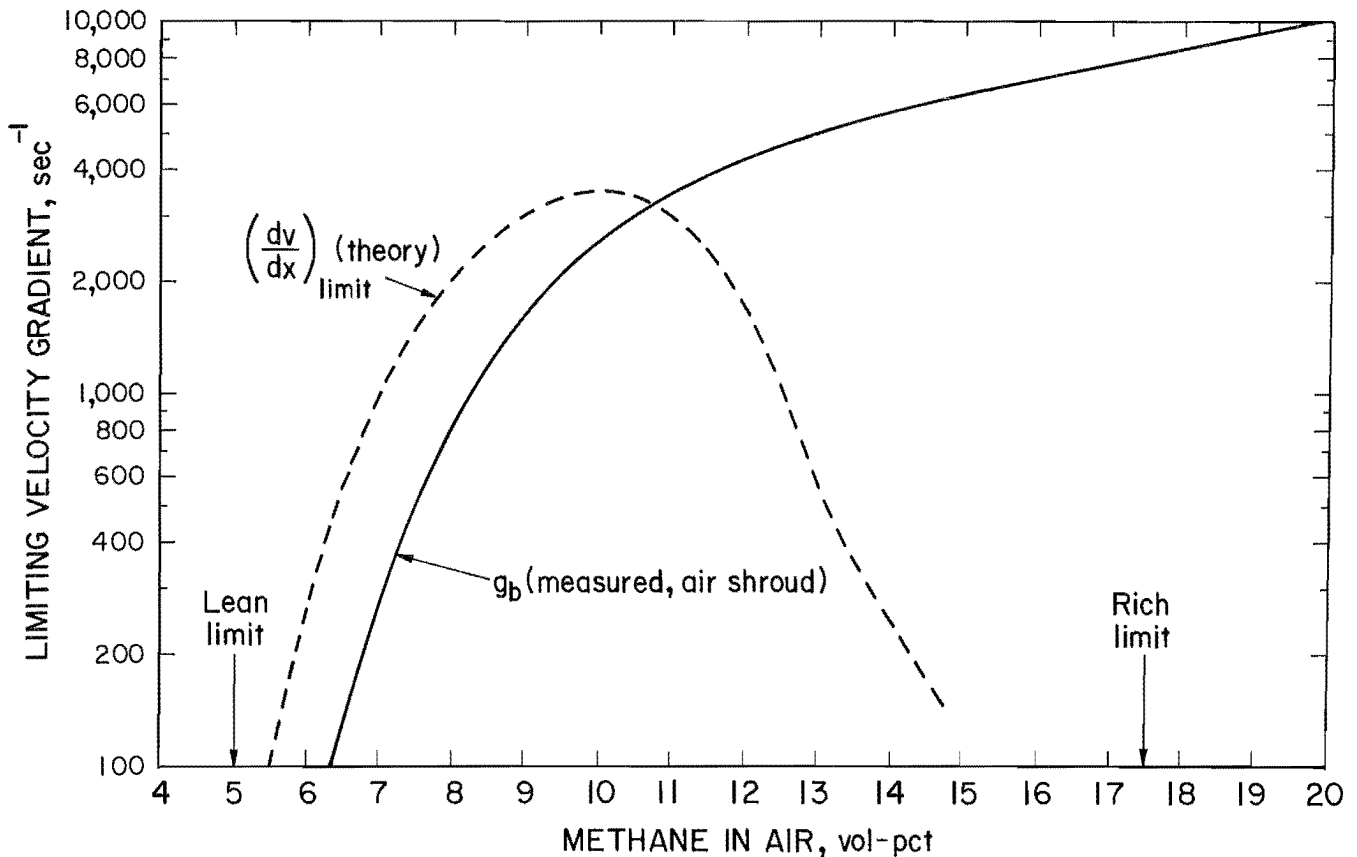


FIGURE 4. - Blowoff limits for premixed, methane-air flames: comparison of data for Bunsen burners in an ambient air environment with theory.

considerations (1-3). While the measured  $g_b$  values shown in figure 4 are about the same order of magnitude as the theoretical predictions, one cannot be too impressed with the different shapes of the two curves. The predicted limit velocity gradient,  $(dv/dx)_{limit}$  (theory), shows the normal, symmetric shape about the near-stoichiometric concentration (10 pct  $CH_4$  in air). That symmetric shape reflects its  $S_u^2$  dependence. Burning velocities peak at near stoichiometric concentrations and drop off symmetrically for lean and rich mixtures. The predicted stretch extinction gradient shows a steeper decline because of its stronger, square dependence on  $S_u$ . By contrast to this symmetric behavior, the measured  $g_b$  curve shows no such symmetry, but climbs continuously with increasing  $CH_4$  concentration. While its slope decreases somewhat for the richer mixtures, the curve continues to rise even at compositions that approach pure methane (10). It must be noted, however, that the rich limit of flammability for methane is 17.5 pct (12). Yet the apparent  $g_b$  data in figure 4 are suggesting that stable flames are being generated for rich compositions that are otherwise determined to be nonflammable. There is clearly a contradiction. How is it possible to observe stable flame propagation in a nonflammable mixture?

One obtains a direct insight into the reason for that apparent contradiction by considering an extreme case: pure methane. Although not shown in figure 4, the apparent, measured  $g_b$  curve does indeed extend out that far and gives a fairly large  $g_b$  value for pure methane. Yet pure methane, in the absence of air or another oxidizer, is entirely nonflammable. Pure methane cannot sustain a deflagration wave. However, if a pure methane stream emanating from a burner tube into an *air environment* is ignited, it will sustain a flame: a diffusion flame. It is that fact or phenomenon that is the source of the apparent contradiction. The  $g_b$  data shown in figure 4 were obtained with an air environment or air shroud around the premixed gas stream. Thus the pure methane data point that is eventually reached does not represent the blow-off limit of a premixed flame but is instead the blowoff limit of a diffusion flame. Such a diffusion flame is not localized near the interior boundary of the tube, nor is its flame front spread across the boundary velocity gradient (as depicted in figures 3D and 3C). The diffusion flame extends over a much larger region above the tube and into the mixing zone between the pure methane stream and the entrained air flow with which it mixes. In this broad diffusion flame region, compositions may vary continuously and velocity gradients decrease continuously from their maximum  $g_b$  values at the interior surface of the tube. Thus both gas compositions and velocity gradients vary together in the broad mixing zone between the fuel stream and the surrounding air. What is the composition of that diffusion flame? It is obviously absurd to attribute a pure methane concentration to such a diffusion flame. That is clearly the source of the confusion and, in that sense, the measured  $g_b$  plot in figure 4 is quite misleading in the rich composition region. The horizontal coordinate in that instance is not a realistic measure of the composition of the unburned mixture entering the flame zone. Even in a diffusion flame, the real concentration in the region where flame propagation is actually occurring is constrained to lie between the lean and rich limits of flammability. Those limits are still controlled by natural convection, which, in the case of a diffusion flame, plays a dual role (13). It is both a quenching process and a promoter of propagation by enhancing the mixing of fuel with the surrounding air. Thus, for the data in figure 4, the flame that is stabilized at apparent methane-air concentrations above the rich limit of flammability is not the premixed flame depicted in a figure 3, but is rather a diffusion flame whose structure is markedly different.

In reality, any rich mixture whose composition is between the stoichiometric value of 9.6 pct methane and the rich limit value near 17 pct methane, will generate a complex, double-flame structure. The double flame consists first of the normal premixed, Bunsen flame similar to that in figure 3B, which is then capped by a

postcombustion diffusion flame. That postcombustion diffusion flame is supported by the excess fuel (and/or its pyrolysis products and partially oxidized intermediates) mixing with entrained air in the regions above the premixed, Bunsen flame. It is because of the presence of that double-flame structure, which eventually transforms into a predominantly diffusion flame at richer concentrations, that the measured  $g_b$  curve in figure 4 continues to rise for rich mixtures rather than to turn downward as the theory requires.

This complexity involving the presence of a diffusion flame can be partially eliminated by replacing the oxidizing air environment by an inert shroud gas. Data for such a system in which nitrogen gas was used as the ambient environment are shown in figure 5. The  $g_b$  data reported by Reed (14) are compared with same theoretical predictions of equation 8. The measured  $g_b$  curve is now as symmetric about the stoichiometric concentration as the theoretical curve. Clearly the anomalous asymmetry caused by the presence of a postcombustion diffusion flame for rich mixtures, is now absent. Rich mixtures flowing into an inert  $N_2$  environment cannot sustain such a diffusion flame.

Although the shapes of the curves are now similar they still differ quite significantly in magnitude. The measured  $g_b$  values are all lower than the predictions of equation 8: from a factor of 4 lower for the lean mixtures to a factor of 2 lower for the rich mixtures. The reason for the difference again involves the surrounding medium. Although that surrounding medium is no longer capable of supporting a diffusion flame, it is still entrained into the premixed stream and dilutes it.

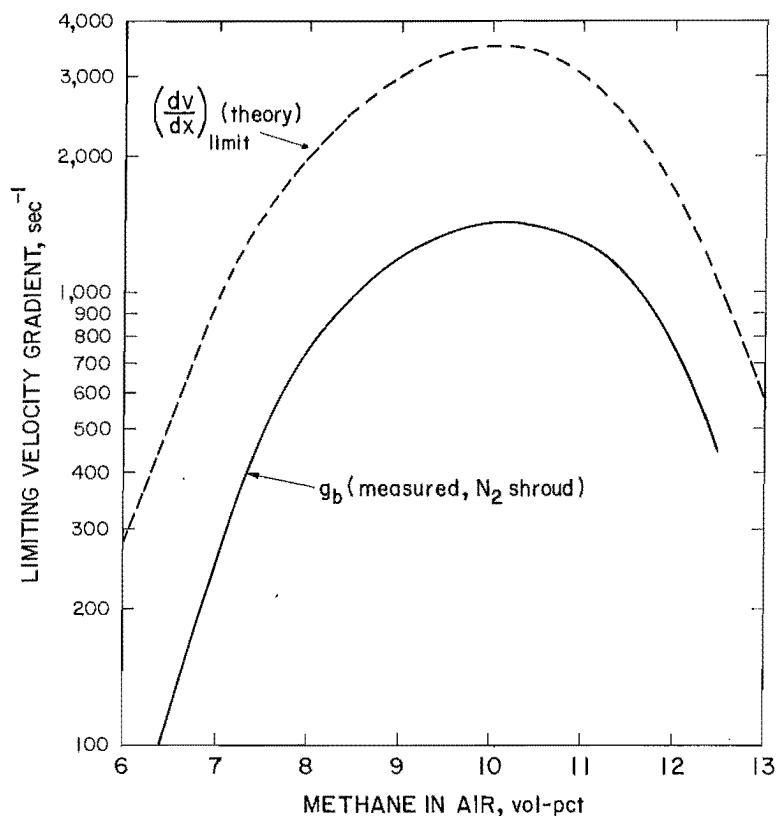


FIGURE 5. - Blowoff limits for premixed, methane-air flames: comparison of data for Bunsen burners in an  $N_2$  environment with theory.

As indicated earlier, in the Poiseuille velocity profile (equation 4), the maximum in the velocity gradient occurs at the inner boundary wall of the tube (at  $r = r_0$ ). It is at that point that a flame of given concentration is stretched to the maximum extent by the flow profile. However, that is also the point at which the premixed gas stream first encounters the ambient  $N_2$  shroud, and where, accordingly, mixing with that ambient gas is most rapid. The entrained ambient medium dilutes the premixed gas stream by pure molecular diffusion and by the convective recirculation eddies that are induced by the shear vorticity of the boundary velocity gradient. As is shown in figure 3B, the Bunsen flame zone stabilizes at some point well above the exit of the tube, so that there is significant opportunity for the entrained medium to dilute the gas stream near the boundary before the unburned mixture enters the flame front.

In the diffusion flame case, that point or mixing edge becomes the "holding edge" of the diffusion flame: the point where fuel and oxidizer mix most readily (13). If the ambient medium contains no oxidizer there can be no diffusion flame; however, there is still mixing at that holding edge or corner. Dilution with nitrogen may not alter the fuel-to-air ratio but it reduces the energy content of the mixture and thus reduces the ideal or intrinsic burning velocity. Accordingly, the real composition of the mixture at the boundary where the velocity gradient is a maximum and where blowoff occurs, is a nitrogen-diluted mixture rather than the mixture whose composition is indicated on the horizontal axis of figure 5. Since the mixture's burning velocity is lowered by dilution, it is not surprising that its measured, limiting boundary velocity gradient is lower than the theoretical value calculated on the assumption that there was no dilution. If the  $(S_u)_{ideal}$  values used to obtain the theoretical curve correspond to methane-air mixtures diluted with 10 to 15 pct excess nitrogen, the two curves would show good agreement. That amount of dilution with entrained nitrogen is quite plausible in the mixing zone at the corner of the emerging unburned gas stream. The dilution occurs before the stream enters the flame front. The actual position at that flame front is well above the exit plane of the burner tube.

#### Inverted Flame

The simplest way to resolve the uncertainty in flame composition caused by entrainment near the region of maximum velocity gradient was suggested by Lewis and von Elbe (6). It involves the use of an inverted flame, which as indicated, should provide a "cleaner test" of the theory (15). In the inverted flame, the boundary that generates the stretch velocity gradient is placed in the *center* of the fuel-air stream rather than at the edge of the stream. The velocity gradient that stretches the flame is thus maximized in the central region of the stream rather than at its boundary with the ambient environment. In the inverted flame, the region of maximum gradient is thus shielded from the surrounding atmosphere by the rest of the gas stream and there is no dilution of composition when the boundary is internal. Accordingly, the initial composition of the premixed, fuel-air stream precisely reflects the real concentration that is approaching the flame front.

Lewis and von Elbe (6) used an internal boundary that consisted of a wire at the exit plane of the tube. A substantial improvement was made by Edmondson, who used a thin plate between two rectangular slotted burners. The plate formed the common, long side between the two rectangular slots through which the gas flowed, and the thickness of the plate was varied (16). The measured  $g_b$  values of Edmondson are shown in figure 6, where they are again compared with the theoretical predictions of equation 8. The three measured curves are for different plate thicknesses. Although the measured curves all have shapes that are parallel to the theoretical curve, the measured  $g_b$  values are now all substantially higher than the predictions of the theory. The fact that the measured results are sensitive to plate thickness is discouraging since it appears to mean that different Karlovitz number correlations pertain to the different plate thicknesses. Dimensionless fluid dynamic correlations should be independent of boundary dimensions. The thinnest plate seems to give the best agreement with theory, and accordingly, Edmondson suggested that "extremely thin stabilization plates should permit the accurate determination of critical values of the Karlovitz flame stretch factor." However, as will be shown, the data already permit such a determination.

The reason for the sensitivity of the data to plate thickness is shown in figure 7. Figure 7 (top), taken from Lewis and von Elbe (6), shows the flow streamlines above a

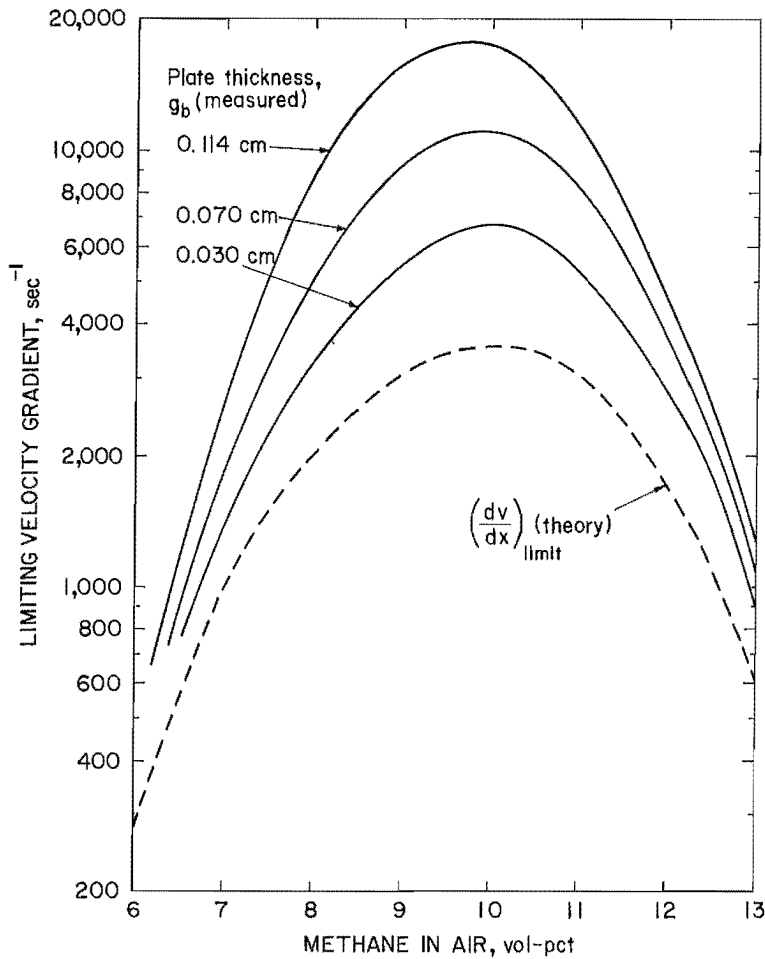


FIGURE 6. - Blowoff limits for inverted, premixed methane-air flames: comparison of data for slotted burners of varying plate thickness with theory.

Figure 7 (bottom) is a similar depiction of the flow streamlines, from such an inverted flame stabilized above a plate boundary. The streamlines and flame front position were drawn from the particle streak photographs of Kawamura (17).

As figure 7 shows clearly, the inverted flame front is stabilized in a diverging flow above the flat end of the boundary wire or plate. The flame front is not located in the gradient *at* the boundary, but is *above* the boundary in the diverging flow. The real velocity gradient at the flame front ( $dv/dx$ ) is therefore always less than the boundary velocity gradient,  $g_b$ , so long as the plate thickness is finite. The thicker the boundary rod or plate, the greater is the flow expansion around the corner and the larger the difference between the real velocity gradient at the flame front and the gradient at the boundary. Thus although the inverted flame solves the problem of dilution of the unburned gas mixture, it does not solve another dilution problem: namely the dilution of the flow gradient by expansion. The boundary velocity gradient within the tube,  $g_b$ , is larger than the actual velocity gradient at the point where the inverted flame front is anchored. Since that anchor point is also the point from which the flame is blown off when a critical gradient is reached, it is not surprising that all the "measured" boundary gradients shown in figure 6 are higher than those of theory. Those measured values are in reality the calculated values within the tube, and not the real values at the anchor points.

thin rod or wire mounted on the axis of a cylindrical tube. The figure shows clearly that although there may be no dilution of composition above the interior boundary of an inverted flame, there is substantial dilution of the velocity gradient. The purpose of the illustration was to show that the inverted flame front depicted in figure 7 (top), induces a back pressure that compresses the recirculation vortex above the flat top of the wire. The illustration was also used to show that velocities were low enough so that there was no eddy shedding of those vortices in the laminar stream. Nevertheless, the figure also shows clearly that the flow streamlines expand as they diverge around the corner formed by the flat end of the wire and its cylindrical surface. More important than the vortex itself, or the absence of shedding, or even the effect of the flame front in diminishing the size of the vortex, is the fact that the flow is *diverging* as it emerges from the interior wire boundary. The magnitude of that divergence is clearly sensitive to the wire or plate thickness, since for an infinitesimally thin boundary there would be neither a vortex nor divergence.

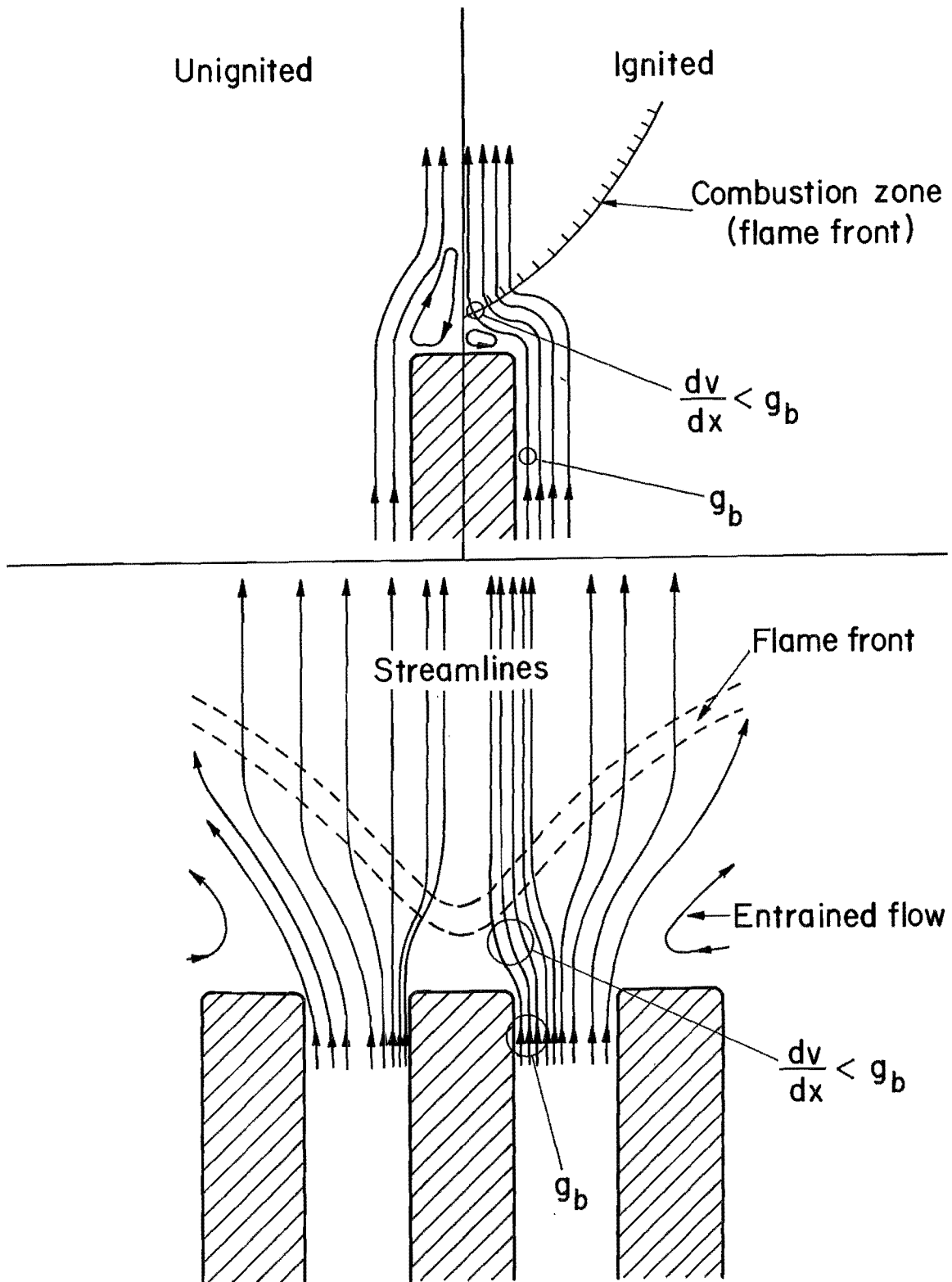


FIGURE 7. - Dilution of the velocity gradient by flow expansion beyond the corner of the interior boundary or holding edge of an inverted flame.

Clearly the simplest way to avoid the washing out or dilution of that gradient by the corner expansion is to have no corner; that is, to have a boundary of infinitesimal thickness. Using the available data in figure 6, that condition can be readily approximated by extrapolating the measured  $g_b$  values to zero wall thickness. That extrapolation is made in figure 8 for several methane-air compositions between 7 and 13 pct methane. Those extrapolated  $g_b$  values are thus a best estimate of what the critical boundary velocity gradient would be for inverted flame blowoff from a boundary of infinitesimal thickness. For such a boundary there is no washing out of the boundary gradient and hence those  $g_b$  values should be a more accurate reflection of the real velocity gradient at the flame front.

Those extrapolated values are plotted as data points in figure 9, where they are again compared with the theoretical predictions of equation 8. Clearly the agreement is now excellent. Thus figure 9, which is only now a "clean test" of the theory, gives virtually perfect agreement.

Thus apart from the well-recognized uncertainties in composition resulting from dilution, one cannot simply assume that the real velocity gradient at the flame front is equal to the boundary velocity gradient in the interior of the tube. Accordingly, the Karlovitz number should not be formulated in terms of  $g_b \delta / S_u$ , but rather in terms of the real velocity gradient. Thus

$$K = \frac{dv}{dx} \alpha / (S_u)_{ideal}^2, \quad (10)$$

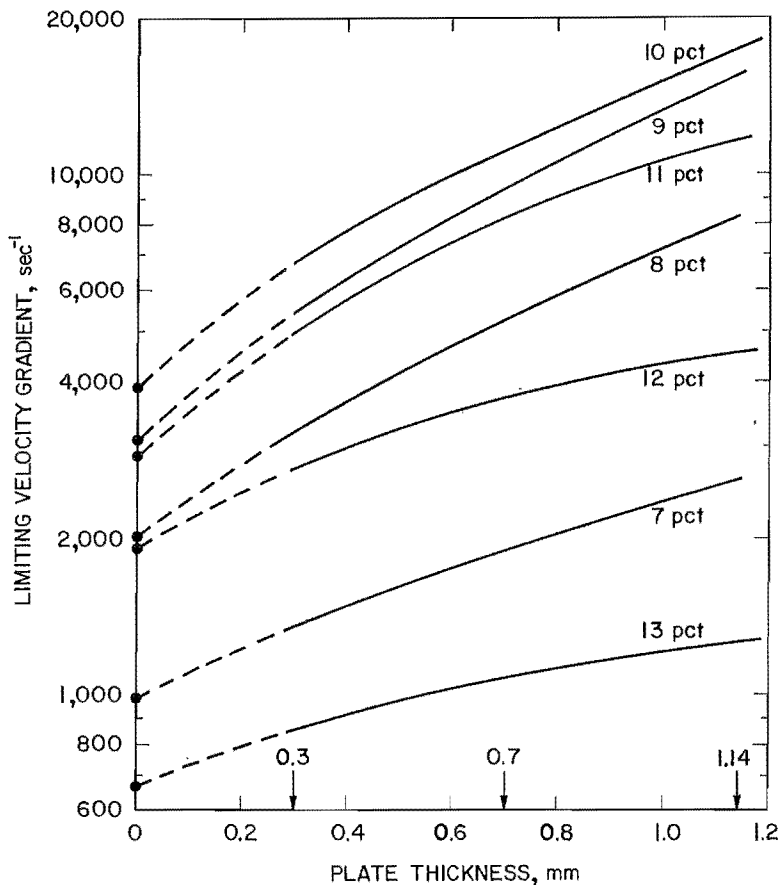


FIGURE 8. - Extrapolation of calculated boundary velocity gradients to zero plate thickness for inverted methane-air flames.

where  $dv/dx$  is the *actual* velocity gradient stretching the flame front and  $(S_u)_{ideal}$  is the *ideal* burning velocity. Considerable confusion has resulted from using the boundary velocity gradient,  $g_b$ , to formulate  $K$ , rather than the real velocity gradient at the actual location of the flame front (16-17).

The excellent agreement in figure 9, which is obtained from the best available data, shows quite clearly that the limit condition for blowoff by flame stretch corresponds quite accurately to a Karlovitz number of unity provided that the number is properly defined. Quite clearly, further validation of the theory is desirable for a wider range of gas compositions, burning velocities, and flow gradients. In view of the past uncertainties and contradictions illustrated in figures 4 through 7, such tests would be fruitless without adequate control of dilution effects. The composition dilution effects resulting from mixing with

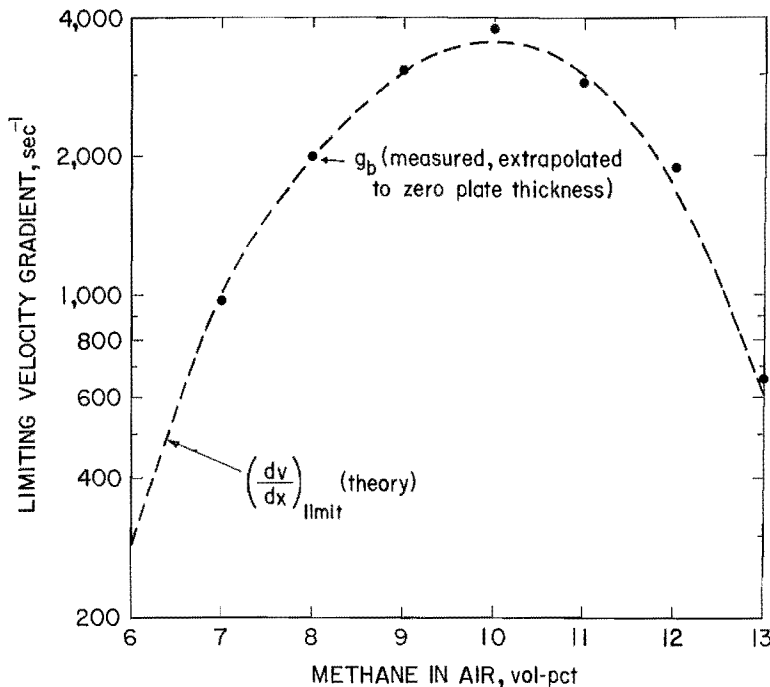


FIGURE 9. - Blowoff limits of premixed, methane-air flames: final comparison of corrected data with theory.

tion. It is rather the "normal" value in laminar, ideal propagation and, similarly, for the burning velocity. The burning velocity that must be used in equation 10 is the ideal, normal or adiabatic burning velocity. It is *not* the actual burning velocity of the stretched flame on the burner that is being used to study its blowoff characteristics.  $(S_u)_{ideal}$  is a function only of the initial thermostatic state of the unburned mixture: its composition, temperature, and pressure.  $(S_u)_{ideal}$ , the convective eigenvalue, is a unique function of the thermostatic state and is entirely independent of flow dynamics. Measured  $S_u$  values can approximate  $(S_u)_{ideal}$  only if they are made under laminar, adiabatic, or ideal conditions. In the presence of flow gradients, measured  $S_u$  values vary and, in fact, at some critical value of  $dv/dx$  they diminish to zero. The failure to recognize that important distinction and to formulate the Karlovitz number properly in terms of  $(S_u)_{ideal}$  values, has led some researchers into considerable confusion and misunderstanding (18).

#### Counterflow Flame

The Bunsen flame and the inverted flame are only two of many possible stretch configurations. Many other flow configurations are possible that generate velocity gradients that stretch flame fronts. A popular configuration during the last two decades has been the counterflow system. It consists of two opposing streams or jets whose flow momenta counterbalance one another and create a stagnation plane between the two streams (19-20). As the streams meet near the stagnation plane, the initial axial momentum of each stream is converted to radial momentum. The axes of the streams are colinear and their intersection with the stagnation plane forms a true stagnation point at which all simple flow components are zero. Moving radially outward from that stagnation point, the flow velocity increases continuously in radial direction. Flames stabilized in or near the stagnation plane are stretched by that radial velocity gradient.

the ambient medium near the stream boundary are most easily resolved by using inverted flames that are shielded from those surroundings. The flow gradient dilution associated with flow expansion around the corner of a boundary can be minimized by using very thin internal boundaries and/or extrapolating the data to zero boundary thickness as was done in figure 8. It is only when such precaution is taken that the actual stretch velocity gradient is equal to the boundary velocity gradient. An alternative, of course, is to measure the actual approaching velocity gradient directly with particle tracking methods or laser doppler velocimeters.

There is one further matter that should be resolved. The flame front thickness,  $\Delta x = \delta = \alpha/S_u$ , to be used in formulating the Karlovitz number is *not* the measured thickness in the stretched condition.

The counterflow configuration was initially used to study the strength and structure of diffusion flames formed by a fuel stream issuing from one tube and an oxidizer stream flowing from the opposing tube. In the counterflow system, the diffusion flame front tends to stabilize near the stagnation plane across which the fuel and oxidizer interdiffuse. Burned products leave the system radially, and reactants are slowed down by their counterbalancing momenta as they approach the stagnation plane. The counterflows must "turn the corner" as they approach one another axially, as reactants, but they then leave, radially, as products. The velocity gradient near the stagnation plane stretches the diffusion flame and eventually extinguishes it at some critical inlet flow velocity of the two streams.

It is important to realize that it is only the simple flow components that are zero at the stagnation point and only the simple component of axial velocity that is zero in the stagnation plane (3). Diffusive flow components are, in fact, a maximum near the stagnation plane and the exact position of the flame front is sensitive to the relative diffusivity of fuel and oxidizer molecules. The effect is not trivial, for as has been shown in a previous study (3), diffusive flow components at a flame front become comparable to simple flow components.

More recently, the same counterflow configuration has been used to study premixed flames. The counterbalancing flows can contain premixed gases of different compositions and the result is a complex, double-flame structure (21). For premixed systems, another variation is to use a solid surface as the stagnation plane. A premixed stream is allowed to impinge on a flat plate whose surface is oriented normal to the initial stream velocity. In that case, a known composition characterizes the gas stream within the interior of the jet and the velocity gradient near the stagnation plane now stretches a premixed flame whose initial composition in the approaching flow is well defined. However, the presence of the flame front induces concentration gradients so that diffusive flow components become comparable to simple flow components near the flame front. If fuel and oxidizer have different diffusivities they diffuse into the flame front at different rates and the effective composition of the reacting mixture may be richer or leaner than the initial composition of the premixed stream, depending on whether the fuel or the oxidizer has the higher diffusivity. The effect, referred to as selective diffusional demixing, has already been considered in detail (3). It is the cause of cellular flame structures and other anomalies in the limit behavior of flames.

In its simplest form, the stagnation-point flow configuration uses a flow stream with an initially flat velocity profile impinging on the stagnation plate. The data of Law (22), obtained with such a stagnation point flow, are shown in figure 10. The best straight-line fit has been drawn through their data points for the stretch extinction limit of their propane-air flames. Actually, two types of flames were observed for various propane concentrations,  $\Omega$ , as a function of initial stream velocity,  $v$ . In the low-velocity region, "rim stabilized" flames are observed. At higher velocities "flat" flames are observed, which, at still higher velocities, are extinguished by the radial velocity gradient near the stagnation plane. The transition region between the rim flames and the flat flames displays the hysteresis effect shown. Whichever flame is initially present tends to persist so that there is always an "overshoot" of the average transition boundary before the actual transition occurs.

The nomenclature used above and in figure 10 does not, however, adequately characterize the true nature of the flames. Both flames are essentially flat flames; the major difference between them simply depends on whether the vertical portion of the rim flame can be maintained near the boundary of the premixed gas flow. The lower

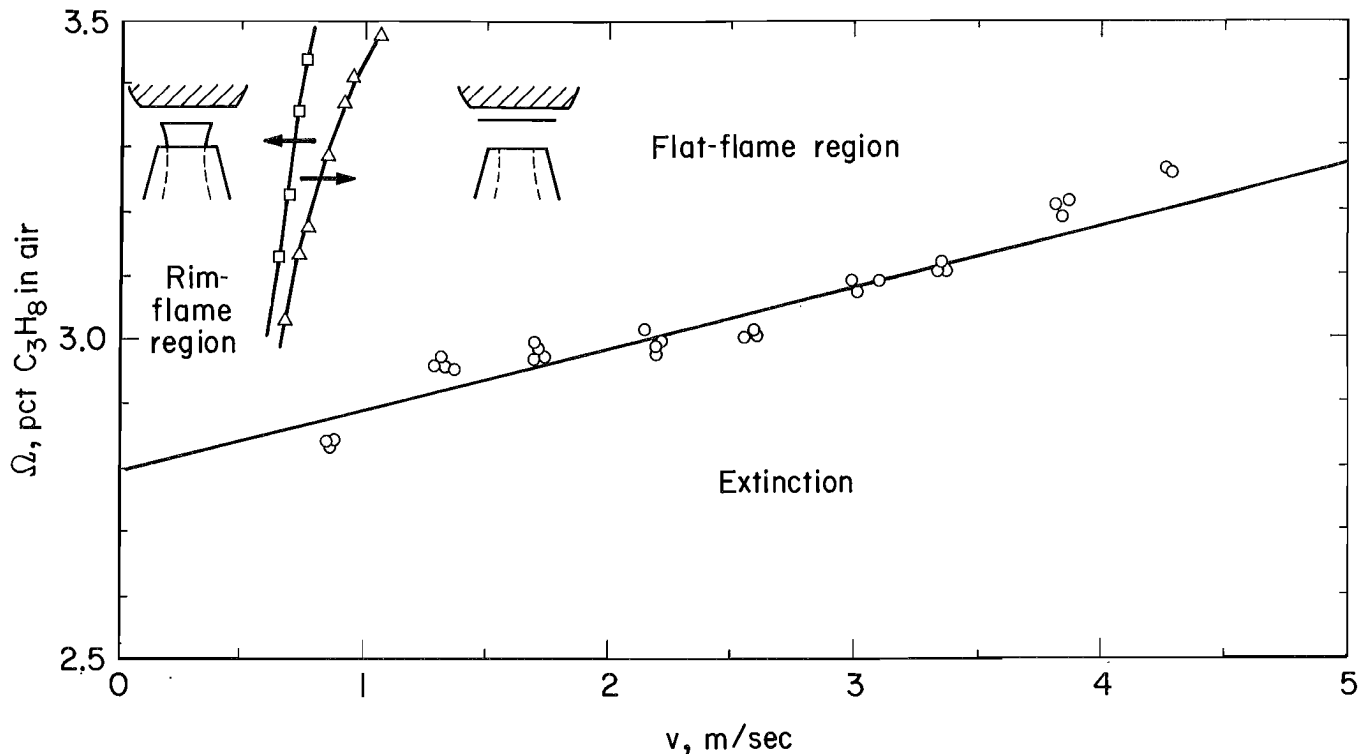


FIGURE 10. - Domains of stability and extinction for premixed normal (rim flames) and for premixed stretched (flat flames) in a stagnation-plate flow configuration.

velocity flame is probably the normal, premixed flame and it is stabilized in the axial stream well below the point where the flow starts to turn the corner. The so-called "rim" flame approximates the normal flat flame depicted in figure 3A, in which the ideal burning velocity in downward propagation is simply balanced everywhere against the flat, axial flow profile. The shape, in this case, is not perfectly flat because of the back pressure induced by the presence of the stagnation plate. That back pressure perturbs the upstream flow profile somewhat. In addition, there are the typical edge effects: entrainment of the surrounding flow and momentum diffusion at the stream-air boundary, which determine whether the vertical portion or rim of the flame can be maintained in the boundary velocity gradient.

As the approach velocity plotted on the horizontal axis in figure 10 is increased, the rim portion disappears and the flame moves upward away from the tube or "burner" and approaches the stagnation plate. As the flame zone moves upward, however, it encounters a decreasing axial velocity component and a changing flow direction from axial to radial. The flow is turning the corner and there is a complex readjustment of propagation directions and burning velocities in the stretched flow field just below the stagnation plate. The new flame that appears at the higher  $v$ -value, the so-called "flat" flame, is in fact a stretched, counterflow flame that is stabilized in the radial velocity gradient as the flow turns the corner. Finally, as figure 10 shows, above some critical inlet velocity, the counterflow flame is stretched to extinction by the radial gradient.

Stretch extinction measurements (23) were reported for both lean and rich propane-air mixtures. The values for the lean mixtures in the stagnation plate configuration are depicted in figure 10. The rich mixture data are complicated by the presence of "corrugated" flames. Those corrugated flames are the "normal" cellular flame structures observed for rich hydrocarbons whose molecular diffusivities are significantly

smaller than that of the oxygen molecule (3). The stretch extinction data for both lean and rich cases, measured by Law (22) and Ishizuka (23) are shown in figure 11, where they are now replotted in terms of the stretch velocity gradient. For the stagnation plate flow system, the radial velocity gradient is the stretch velocity, and it is given by  $dv/dr = dv/dx = v/2\ell$  where  $\ell$  is the distance between the nozzle exit plane and the stagnation plate. Ishizuka (24) has also reported more recent data in a range of much lower velocity gradients, using a counterflow configuration between two nozzles. For the counterflow configurations, the stretch velocity gradient is  $dv/dr = v/\ell$ . Those data are also shown in figure 11. Their measurements

are compared with the predictions of equation 8 based on the best available  $(S_u)_{ideal}$  values for propane-air (4). Also shown, for comparison purposes, is the standard blowoff curve for propane on a Bunsen burner in an air environment.

The stagnation plate and counterflow systems provide the experimentalist with an opportunity of studying flame stability and blowoff limits at much lower stretch gradients than is possible for Bunsen flames or inverted flames in tubes. Although velocity gradient extinction limits are shown in figure 11 for both lean and rich mixtures, the rich mixtures are complicated by the presence of the selective diffusional demixing process. That process (3) generates "cellular," "corrugated," or "star-shaped" flames. Such cellular structures complicate the comparison between theory and experiment partly because their presence makes it difficult to obtain accurate measurements for  $(S_u)_{ideal}$  in the rich region. There are additional complications related to the fact that the selective diffusional demixing process generates concentration gradients. As a result, the real fuel concentrations entering the flame front vary periodically in the direction normal to the unburned gas blow. Thus a single value for  $(S_u)_{ideal}$  can no longer be used to characterize the entire flame front. For lean mixtures, however, there are no cellular flame structures in propane-air mixtures. The selective diffusion of the higher diffusing oxygen

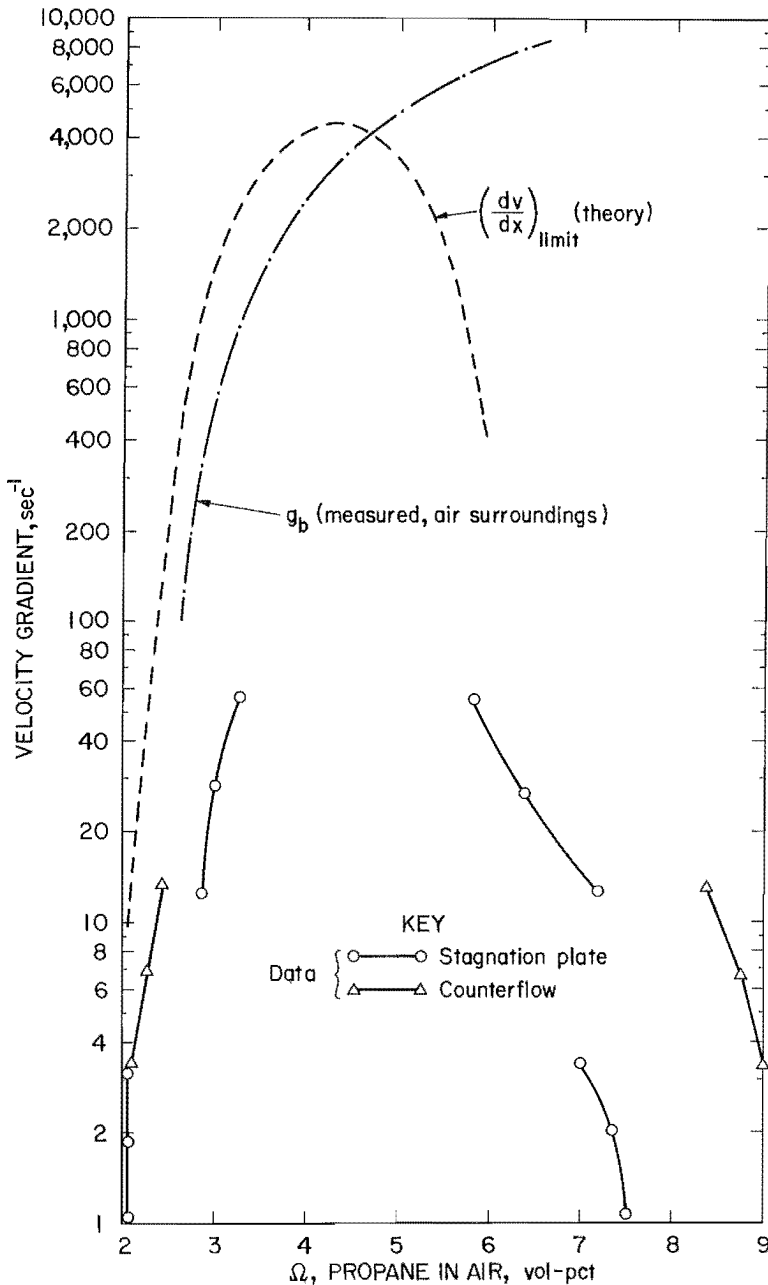


FIGURE 11. - Blowoff (extinction) limits for premixed propane-air flames in counterflow and stagnation plate flow configurations compared with theory and with normal blowoff limits for Bunsen flames in air.

molecule still occurs; however, the process stabilizes laminar structures in the lean region. Thus accurate  $(S_u)_{ideal}$  values are available for the lean mixtures of propane in air.

The comparison of the measurements of Ishizuka (23-24) with the theoretical curve in figure 11, shows that the measured values generally fall below the theoretical curve. One should remember, however, that in those composition ranges near the limits of flammability, the inlet gas flow velocities are quite low, and comparable to the limit burning velocities for quenching by natural convection (1-3). When the inlet flow velocities are as low as 3 to 9 cm/sec, the real velocity gradients are no longer those calculated from the inlet flow,  $v$ , and the nozzle-to-plate distance,  $\ell$ . Instead, buoyancy induced flows become comparable to inlet flows, and eventually they can dominate near the natural extinction limit. Thus one suspects that the measured  $g_b$  values are below the calculated ones because there is an additional buoyancy-induced velocity gradient that must be added to  $g_b$  in order to obtain the true value of  $dv/dx$ . In a flow that contains both the forced flow gradient ( $g_b$ ) and that natural (buoyancy-induced) flow gradient, both components are required in order to obtain the true value of  $dv/dx$ . It is only the forced component that is given by  $dv/dr = v/2\ell$  (or  $v/\ell$  for two counterflowing streams). The natural component is not an externally controllable variable, but it is nevertheless an integral component of the flow field. Only direct measurements of the actual velocity gradients can reveal its magnitude.

#### NORMAL LIMIT FOR UPWARD FLAME PROPAGATION: FLAME STRETCH UNDER NATURAL CONVECTION

It is now time to focus in more detail on that natural convective flow component. It was argued in previous publications (1, 12-13, 25) that the "normal" limit of flammability, as typically measured and tabulated (26-27), is in effect a limit induced by natural convection. The limit compositions, whether measured in upward, downward, or horizontal propagation, reflect the competition between two forces: the combustion force and the buoyancy force. Each force generates different motions in the gas ahead of the flame front and the motions induced by the buoyancy force limits the ability of the flame to propagate in the unburned gas mixture. It was argued that flame extinction in upward propagation is caused by the ascendance of the buoyancy force operating through the mechanism of flame stretch. Because of natural convective flows, generated by buoyancy, upward propagation always occurs into a velocity gradient in the cold gas, and at some low but finite propagation rate, the flame is simply blown out by its own buoyancy-induced flows. In this section, this question is considered in more detail.

#### Maximum Buoyant Rise Velocity for Spherical Propagation

It is possible to obtain some reasonable insight into the nature of the buoyancy force, and the effect it may have on the flow structure, by considering the simplest example: an idealized, spherical combustion wave propagating into a premixed gas of uniform composition in a gravitational field.

The absolute buoyancy force on each unit volume of gas of density  $\rho$  is simply  $\rho g$ , where  $g$  is the normal gravitational acceleration. If a gas is of uniform density  $\rho$ , in a constant  $g$  field, the gravitational force is everywhere constant at  $\rho g$  and there is no net gravitational force on the gas. That is the case for an isothermal volume of gas or air of constant composition near the surface of the earth. However, the normal combustion process that occurs after the ignition of an exothermic mixture is irreversible, and generates burned gas at a density,  $\rho_b$ , which is normally much lower

than the density of the unburned mixture,  $\rho_u$ , from which it was generated. Thus with a burned gas density  $\rho_b$  behind a flame front, and an unburned gas density  $\rho_u$  ahead of a flame front, there is a net gravitational force couple,  $(\rho_u - \rho_b)g$ , across the flame front. There is thus a force gradient that induces convective flows, and flame propagation in those buoyancy-induced flows inevitably produces distortions in flame shape (12).

In the simplest idealization, the details of that distortion are ignored and one focuses on the overall buoyant rise velocity of a spherical ignition kernel that is assumed to propagate spherically as its center of mass responds to the net buoyancy force.

That idealized situation is depicted in figure 12. At some initial time,  $t$ , a fireball of radius  $r(t)$  is rising upward by buoyancy at a velocity  $v(t)$ . At some time  $t + \Delta t$  later, the fireball has expanded to a new radius  $r + S_b \Delta t$ , and its new buoyant rise velocity is  $v(t) + (dv/dt) \Delta t$ . The quantity  $S_b$  is the spherical flame speed relative to the laboratory observer. The buoyancy force acts simultaneously on both the burned product fireball and the unburned reactants that surround it. The momentum change induced by buoyancy must involve not only the upward motion of burned

products, but also the simultaneously induced downward motion of the unburned gases, since the cold surroundings must descend to fill the space vacated by the fireball. An equivalent volume of the cold surroundings is also idealized and shown in figure 12A. It is depicted as separated from the fireball, expanding in size as the fireball does, and descending at an identical velocity. The left hemisphere of the fireball moves upward as its surroundings descend, introducing a moment of force or torque about the equatorial axis, which generates a continuous cyclonic vorticity about the rising fireball. The same motions occur in the right hemisphere, which generates a continuous vorticity that is anticyclonic. Since these motions of fireball and surroundings are coupled, and involve a moment of force or torque, they are referred to as being induced by the buoyancy force couple.

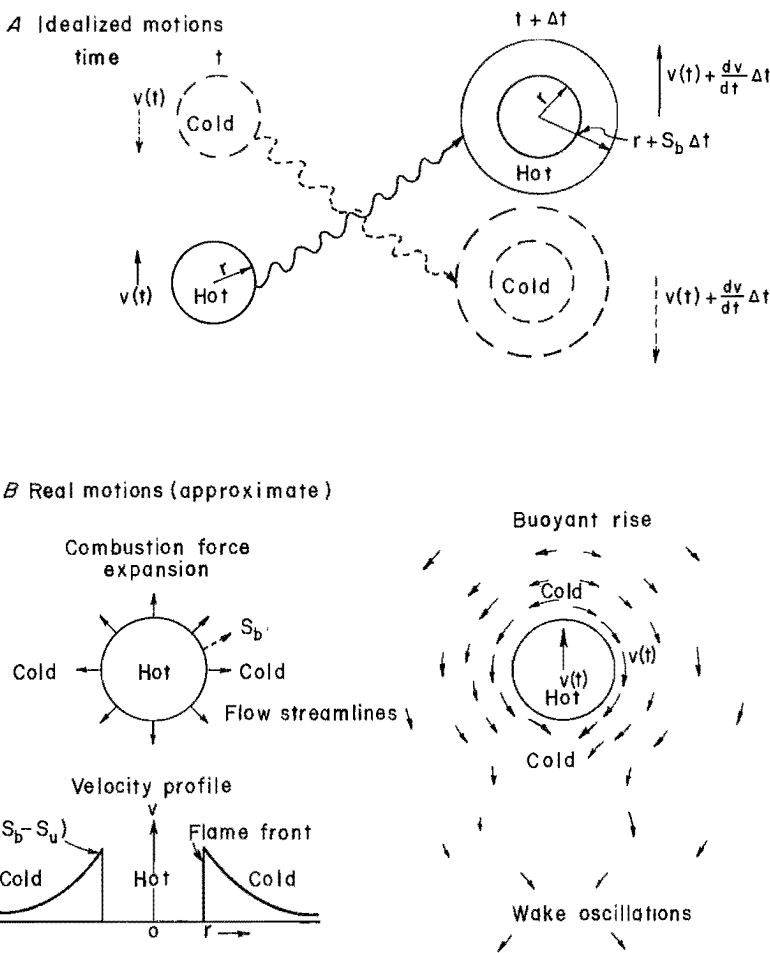


FIGURE 12. - Idealized motions (A) and approximate real motions (B) during the buoyant rise of an outward-propagating, spherical, flame kernel under the simultaneous influence of the combustion force expansion and the buoyancy force couple.

In reality, the motion of the surroundings is necessarily more complex, and this is depicted in figure 12B where the motions are viewed in a coordinate system moving upward with the fireball. There is first a continuous outward motion induced by the combustion

force expansion. At the flame boundary, the unburned gas recedes at a velocity  $S_b$  ( $1-\rho_b/\rho_u$ ) and this radial velocity decreases with the inverse square of the dimensionless distance from the center of the fireball. Superimposed on this expansion are the buoyancy-induced flows. Near the top of the fireball the surroundings must move outward, parting from the upward path of the fireball. In the equatorial regions, the motion of the surroundings is downward as required by the buoyancy force couple. Near the bottom of the fireball, the surroundings move inward in order to fill the space being vacated by the bottom of the rising fireball. In the idealization of figure 12A, it is assumed that the buoyancy component of the outward motions at the top, and inward motions at the bottom, are canceled exactly, so that no other motions are induced but those necessary to raise the expanding fireball upward at  $v(t)$  and to simultaneously displace an equal volume of the surroundings downward at the same velocity. Any additional buoyancy-induced motions that appear either with the fireball or in the surroundings (as in a wake) should be treated as a drag force that would retard the rate of rise. Accordingly, it is possible to derive an equation for the maximum buoyant rise velocity in initially stationary surroundings (13). That maximum value, which is a quite accurate approximation for the measured rise velocities of fireballs of small to moderate dimensions (12), is given by

$$v_b(t) = \left[ \frac{1}{1 + 3 \left( \frac{\rho_u}{\rho_u + \rho_b} \right)} \right] \left[ \frac{\rho_u - \rho_b}{\rho_u + \rho_b} \right] gt, \quad (11)$$

where  $v_b(t)$ , the buoyant rise velocity, is a linear function of the time,  $t$ . For spherical propagation, one has  $t = r(t)/S_b = r(t)\rho_b/\rho_u S_u$ .

A more precise consideration of the problem of flame stretch for flows induced by the simultaneous interaction of buoyancy and spherical propagation awaits a more accurate description of the real flow field than has heretofore been available in the literature. Clearly, the real field is a complex, time-dependent structure that reflects the sum of the motions depicted in figure 12B. An attempt will be made to estimate that real flow field in a following section.

#### Recent Estimates and Observations of Buoyancy-Induced Limits

Estimates of the limit burning velocity for flame stretch quenching have recently been presented by Hertzberg (1, 12, 25). A simple force balance argument was made as follows. The motions induced by a propagating flame originate in the combustion force. That force is responsible for the outward motions depicted in the left portion of figure 12B. That internal force is equal to the gradient of the kinetic energy increase per unit volume across a propagating flame zone.

$$\text{Combustion force} = \frac{\Delta(\text{KE})}{\Delta x} = \frac{1/2 \rho_b S_b^2 - 1/2 \rho_u S_u^2}{\alpha/S_u} = \frac{S_u^3}{2\alpha} \frac{\rho_u}{\rho_b} (\rho_u - \rho_b), \quad (12)$$

where  $x$  is the propagation direction. However, product gases are less dense than reactants and their generation induces natural convective flows that compete with combustion-induced flows. The competition dissipates power from the combustion wave. Those convection flows for spherical propagation are depicted in the right-hand portion of figure 12B. The competing force is the buoyancy force couple whose magnitude is given by

$$\text{Buoyancy force} = (\rho_u - \rho_b)g. \quad (13)$$

One associates the average convective flow conditions with the horizontal propagation condition, and assumes that a horizontal propagation limit is reached when the

two competing forces are in balance. Equating equation 12 with 13 defines a limit burning velocity for horizontal propagation of

$$(S_u)_a = \left[ 2 \alpha g \frac{\rho_b}{\rho_u} \right]^{1/3}. \quad (14)$$

Substituting a consistently used value of  $\alpha = 0.55 \text{ cm}^2/\text{sec}$  for the effective diffusivity, setting  $g = 980 \text{ cm}/\text{sec}^2$  for the gravitational acceleration at the earth's surface, and using a typical density ratio for near limit conditions of  $\rho_b/\rho_u = 1/5$ , gives  $(S_u)_a = 6.0 \text{ cm}/\text{sec}$ . This limit velocity for horizontal propagation has already been shown to give realistic predictions for the lean limit concentrations for a wide variety of fuels (1, 12).

There is an expectation, implicit in the above derivation, that burning velocities do not simply diminish continuously toward zero as the flammability limits are approached. Rather, one should expect that propagation should be quenched discontinuously for composition whose ideal velocities are equal to or less than  $(S_u)_a$ . LeChatelier and his colleagues in their pioneering researches, had in fact noted that burning velocities extrapolated to finite values at the limit compositions. Egerton (28) had noted that a satisfactory theory should be able to predict both the burning velocity at the limit and the limit concentrations. Linnett (29) showed that the factor that seemed to be most invariant for many fuel-air systems was the limit burning velocity. Levy's (30) optical studies of limit behavior showed the significance of buoyancy effects. Dixon-Lewis (31-32) concluded, based upon experimental studies of slow flames stabilized well below their conventional limits, that the flammability limits were determined largely by convective gas velocities.

More recently, Hertzberg approximated the maximum velocity gradient in buoyancy-induced cold gas flow above a rising, spherical flame kernel by

$$\frac{dv}{dx} \approx \frac{3}{2} \frac{v_b}{r}. \quad (15)$$

If equation 15 is substituted into equation 7 and the resultant equation is combined with equation 11, one obtains

$$\begin{aligned} (S_u)_{a, \uparrow} &\approx \left[ \frac{3}{8} \left( \frac{\rho_u - \rho_b}{\rho_u + \rho_b} \right) \alpha g \frac{\rho_b}{\rho_u} \right]^{1/3} \\ &\approx \left[ \frac{3}{16} \frac{\rho_u - \rho_b}{\rho_u + \rho_b} \right]^{1/3} (S_u)_a \approx \frac{1}{2} (S_u)_a. \end{aligned} \quad (16)$$

The functional form of equation 16 is identical to that of equation 14 even though the latter was obtained by an entirely independent force-balance argument. The derivation of equation 16 thus gives a limit burning velocity for upward propagation that is approximately half the value for horizontal propagation. Although the geometry of the problem was considered in an idealized way in the derivation of equation 16, the final result turned out to be independent of any geometric factors. In the derivation of equation 14, no detailed considerations of geometry were made, only a force balance agreement was used; and yet essentially the same result was obtained.

In the next section, the geometry of the problem of upward flame propagation will be considered in more detail.

Let us first, however, review some of the more recent experimental studies that have dealt with the problem of buoyancy-induced flame stretch. Diffusion flames from

laminar gas jets in air were studied in a centrifuge at elevated gravity levels by Altenkirch (33). With increasing  $g$  levels, the diffusion flames would tend to move away from the burner rim and lift. Higher  $g$  levels led to pulsation of the diffusion flames and eventual extinction. For the methane, ethane, and propane flames that were studied at moderate to low jet velocities, the lifting and extinction process correlated reasonably well with the dimensionless group,  $g\alpha/S_u^3 = \text{constant}$ . Comparison with equations 14 and 16 show clearly that the same dimensionless group is involved. The comparison however suggests that the dimensionless constant is simply related to the expansion ratio,  $\rho_u/\rho_b$ . The centrifuge data gave absolute  $g$  values for lift-off and extinction that were in the range of 10 to 30  $g_0$ , where  $g_0$  is the earth's gravitational acceleration ( $g_0 = 980 \text{ cm/sec}^2$ ). From equation 16, the predicted  $g$  value for the extinction of a stoichiometric, premixed hydrocarbon flame in upward propagation is about 4,300  $g_0$ . The reported values for the diffusion flames of Altenkirch (33) are much lower because diffusion flames involve near-limit compositions in the mixing zone between the fuel stream and the entrained air stream (13). If one uses near-limit burning velocities for horizontal or downward propagation of 6 to 8 cm/sec, equation 14 predicts extinction values at  $g$  levels of 10 to 30  $g_0$ . Those are, in fact, the values observed for the diffusion flames.

In a recent study of premixed flames under earth's gravity, von Lavante (34) investigated the mechanism of extinction for upward propagating methane-air mixtures at lean limit compositions. Tubes of various diameters were used and it was observed that both the flow field and the flame shape near the limits were governed mainly by the effects of buoyancy. These observations confirmed those of Levy (30) who had showed that in upward propagation, the flame fails first at the center of the tube. That is precisely the point at which the flame is stretched the most by the buoyancy-induced flow field. Further, von Lavante presented an approximate solution to the flow field in the unburned gas and used the solution to calculate the Karlovitz numbers. The calculated Karlovitz numbers were of the order of unity at the centerline of the tube as the extinction limit was approached. Thus, it was concluded that flame stretch was the primary extinction mechanism for upward propagation. The tube dimensions varied from 5 to 20 cm in diameter. Wall heat flux measurements were also made and those measurements further confirmed that wall losses were not significant in the extinction process within those relatively large tube dimensions.

#### Flow-Field Solutions for Spherical Propagation in Buoyancy-Induced Flows: Flame Stretch Limit for Upward Propagation

Consider now, in more quantitative detail, the real flow field in the upward propagating hemisphere of a spherical flame front. The spherical, outward expansion of the flame front induces expanding radial motions that are driven by the combustion force. Simultaneously, the fireball rises under the influence of the buoyancy force-couple as the cold surroundings descend. A qualitative picture of those two motions, considered independently, was depicted in figure 12B where flow streamlines were shown in a coordinate system moving upward at the buoyant velocity of the fireball. The very top of the upper hemisphere of the spherical fireball kernel propagates upward into a cold gas stream whose initial approach velocity is downward in that coordinate frame. The cold gas stream then diverges or parts into two equal streams whose motions in the equatorial regions are now parallel to the flame front. In those equatorial regions they resume their downward flow; however the flame front is now propagating outward. Those streams are no longer flowing into the propagation direction but are now flowing perpendicular to the propagation direction. The approach flow, which diverges and deflects around the spherical kernel, thus stretches the flame front in much the same way that it is stretched in the counterflow configuration near a stagnation plate. That counterflow system was discussed in the previous section. Here, the spherical case is to be considered.

If, at any instant, one freezes the combustion force expansion motion, the flow field in the unburned gas induced by the buoyant rise velocity,  $v_b(t)$ , should be similar to that around a rising spherical balloon. One chooses a coordinate system moving upward with the buoyant velocity,  $v_b(t)$ , and assumes that the motion of the surroundings adjusts instantaneously to that buoyant velocity so that it may be approximated by parallel flow past a sphere. It is thus assumed that the buoyancy-induced component of the flow field is that of classical Stokes flow past a sphere caused by a free stream velocity,  $v_b(t)$ , which adjusts instantaneously to buoyant velocity vector. The classical Stokes flow solutions (35) are

$$v_r = -v_b(t) \cos \theta \left[ 1 - \frac{3}{2} \frac{r_0}{r} + \frac{1}{2} \left( \frac{r_0}{r} \right)^3 \right] \quad (17)$$

and

$$v_\theta = v_b(t) \sin \theta \left[ 1 - \frac{3}{4} \frac{r_0}{r} - \frac{1}{4} \left( \frac{r_0}{r} \right)^3 \right], \quad (18)$$

where  $r$  is the radial distance from the center of the sphere,  $r_0$  is the diameter of the sphere,  $\theta$  is the polar direction, and  $v_r$  and  $v_\theta$  are the radial and tangential (polar) velocity components. A typical set of those Stokes flow velocity vectors are depicted in figure 13.

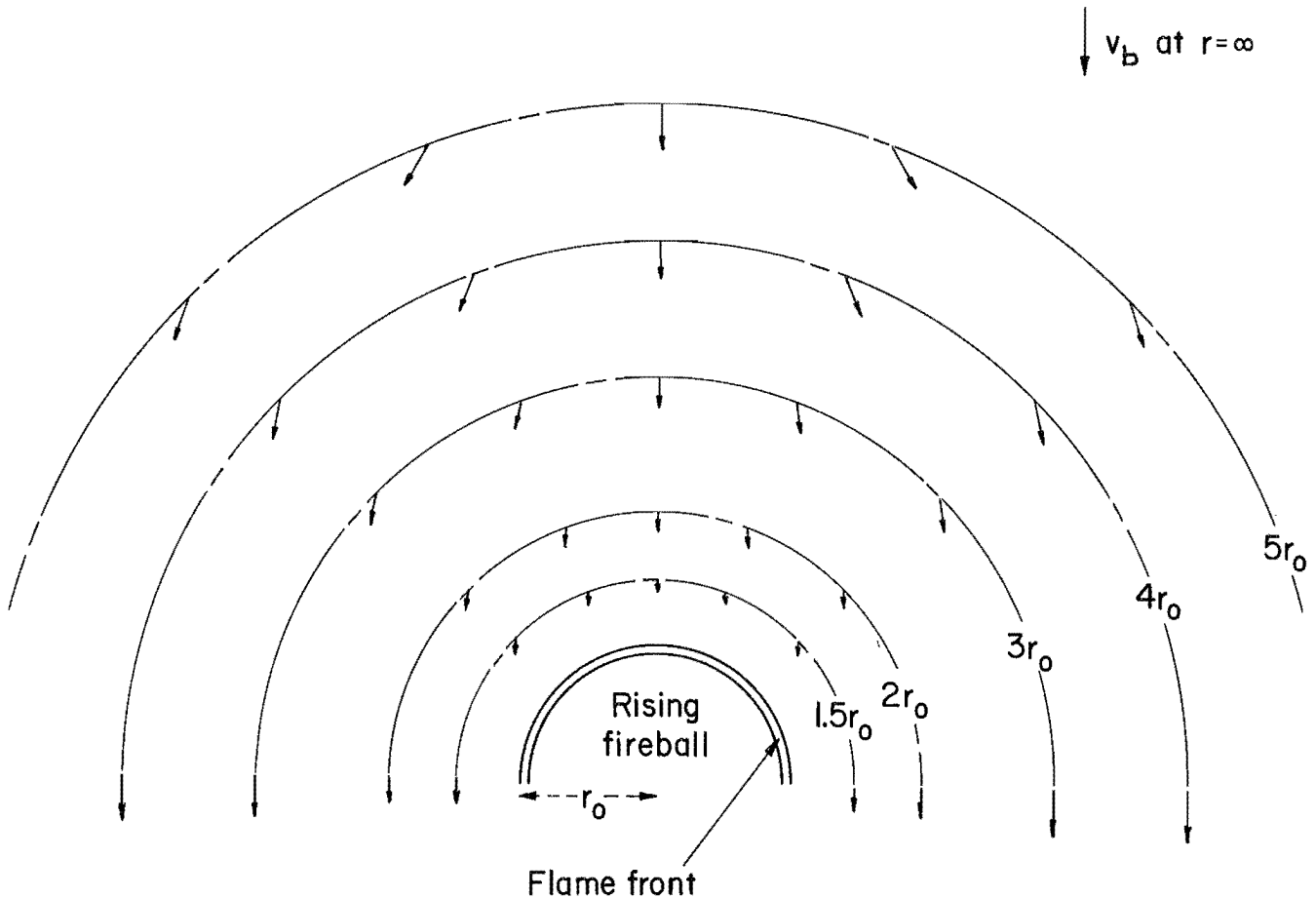


FIGURE 13. - Buoyancy-induced, flow-field vectors of the unburned gas around a rising, spherical flame kernel from the classical Stokes flow solutions past a sphere.

It is important to recognize that the "streamlines" that were depicted in figure 12B are not as realistic a representation of the real flow field in the boundary layer near the sphere as are the velocity vectors shown in figure 13. In any two-dimensional projection of stream lines, such as is attempted in figure 12B, there is an inevitable convergence of those streamlines in the flow passing the sphere, which incorrectly implies an increase in velocity. In reality the flow field just above the balloon or fireball is decelerated and deflected or diverted into "two" streams that flow around the sphere as shown the two-dimensional projection of figure 13. Any new flame surface appearing at the top of the fireball as it propagates upward is thus stretched in the diverging flow gradient moving to the right and to the left of the sphere. The unburned gas approaching from above to form that new flame surface has been "turning the corner" to flow around the sphere, and hence it is "stretched" as it enters the flame front to react. Although the fireball is not a solid sphere of infinite viscosity relative to the gas, it is nevertheless at such a higher temperature and therefore so much more viscous than the unburned surroundings, that any "slipping" or "sliding" of the boundary is minimal. Any such slip in the fireball boundary would appear as an induced flow or internal vorticity within the fireball. It would act as an additional drag force to reduce  $v_b$  somewhat and would also reduce the stretch gradient. For the temperature differences involved, that slip effect will be neglected to first order. Thus, as shown in figure 13, cold gas approaches the top of the flame kernel with a buoyancy-induced approach velocity,  $v_b(t)$ , which is initially radial at  $\theta = 0$ . As it approaches further, it is deflected in the polar,  $\theta$ -direction by the spherical kernel. By the time it passes the equator of the kernel, its radial component is zero and its buoyancy-induced velocity is entirely tangential.

Apart from the question of slip, the "boundary" is not a solid surface at which flow velocities are zero. Rather, it is an outward moving boundary that generates an outward radial flow in the unburned mixture as indicated in figure 12B. The boundary overtakes that outward flow at the burning velocity,  $S_u$ .

In a first approximation to the dynamics of that part of the problem, it is assumed that an element of cold gas that approaches the upper hemisphere of the flame front from above (and which is met by that front as it expands) has a finite "residence time" during which it can react with, and contribute its energy to, the flame front. That interaction time or residence time near the approaching flame front is directly proportional to the circumferential distance the cold gas travels before it leaves the interaction zone. The residence time is inversely proportional to the velocity with which the cold gas flows around that zone. Since the tangential velocity with which the unburned gas flows around the zone is approximately  $v_b$ , and the distance of travel near the upper hemisphere is one-quarter of the circumference, one has

$$\tau_r \approx \frac{\pi r}{2 v_b} \quad (19)$$

The residence time is clearly limited by the buoyancy-induced, convective flow gradients depicted in figure 13. Now, the characteristic time for the completion of the combustion reactions within the flame front is  $\tau_{pm} = \alpha/S_u^2$ . As previously indicated, the ratio  $\tau_r/\tau_{pm}$  is, in effect, the Damkohler number for the flame front. If the residence time is too short, new volume elements of unburned gas passing into the flame front cannot be activated to reaction during the necessary reaction time,  $\tau_{pm}$ . The flame is then "forced to swallow" more unburned gas than it can handle in the time available. New flame surface is created at too fast a rate and the flame is "stretched" beyond its limit. That is, it is "blown off." In this case it would be

blown off by its own buoyancy-induced flow field. The limit condition is obtained by setting  $\tau_r = \tau_{pm}$ .

Substituting equation 11 into equation 19 with the limit condition of unity Damkohler number gives a result that is virtually identical to equation 16. As indicated earlier, this Damkohler number approach is an equivalent way of looking at the flame stretch phenomenon.

A somewhat clearer picture of the detailed geometry of the problem can be obtained by adding the two types of motions as though they were independent. To the buoyancy-induced flow velocities depicted in figure 13, one adds the radial motions induced by the combustion force expansion. For spherical propagation outward from a point source, in the absence of buoyancy, the unburned gas velocity is everywhere radial and is given by

$$v_r(r) = S_u (\rho_u/\rho_b) (1 - \rho_b/\rho_u) \left(\frac{r_0}{r}\right)^2. \quad (20)$$

If one makes the assumption that the resultant flows under the influence of both combustion and buoyancy forces are the simple vector sum of the flows from each force acting independently, it is possible to add the combustion-induced radial vectors of equation 20 to the buoyancy-induced vectors already plotted in figure 13, and which were obtained from equations 17 and 18. The resultant vector sum for the motions induced by both buoyancy and combustion process are plotted in figure 14. In the plot

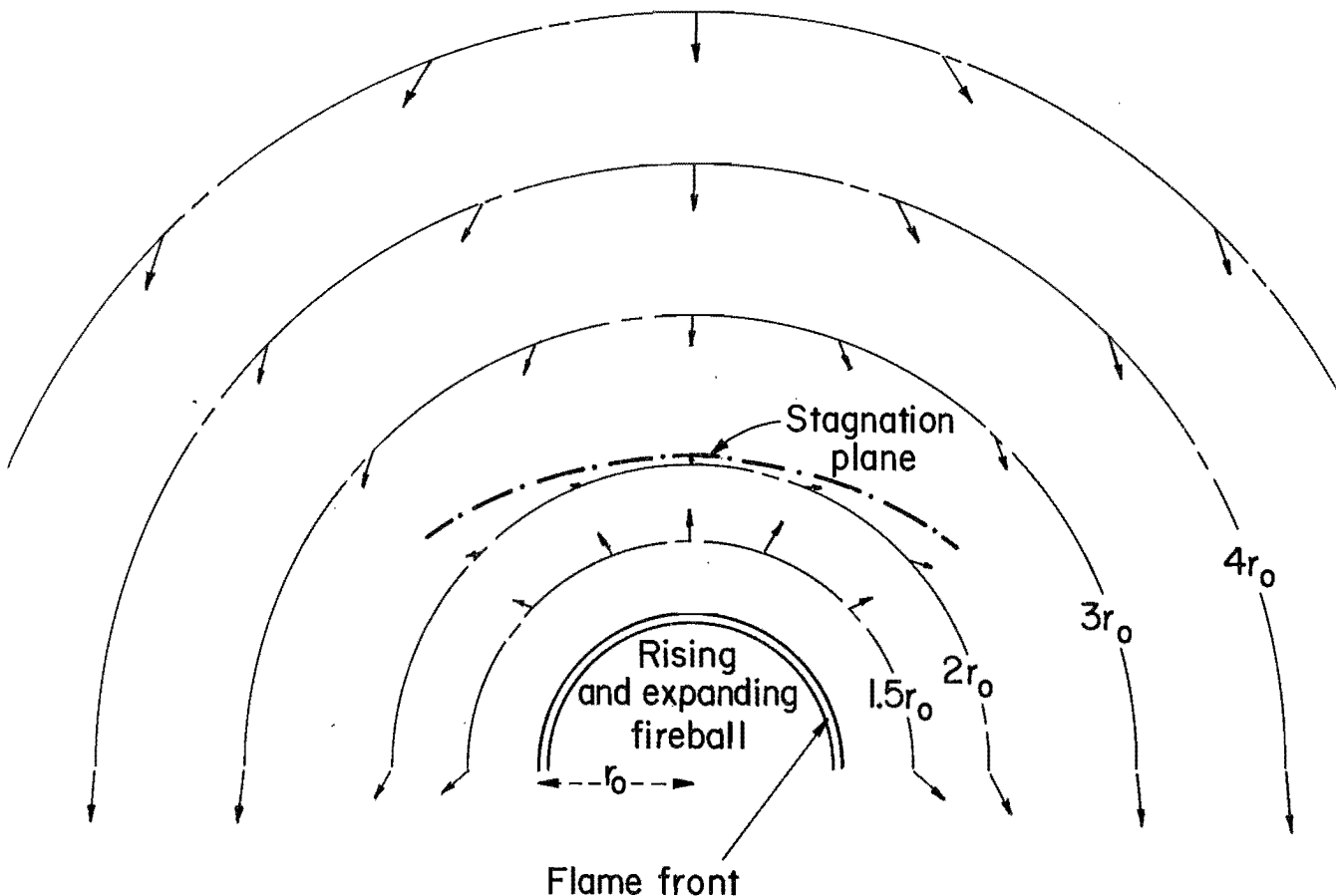


FIGURE 14. - Simple vector sums of combustion force expansion flow field and the buoyancy-induced Stokes flow field, assumed to be operating independently in steady state.

shown it has been assumed that the fireball size is such that  $v_b \approx 3 S_u$ . Clearly, adding the combustion force motions to the flow field moves the stagnation point away from the surface of the sphere. In figure 14, the stagnation point is located near  $r = 2r_0$ . The flow is clearly that of a counterflow configuration. The downward flows approaching the flame front from above must "turn the corner" as they approach the stagnation plane. Similarly, the flows moving upward from the expanding and propagating flame front must also "turn the corner" as they approach the stagnation plane. The stagnation plane is depicted as the chain-dashed line in figure 14. Although the flow is clearly similar to the counterflow configuration, the stagnation plane is no longer flat. Instead it is curved to match the curved source of spherical flow.

The higher the ratio of buoyant velocity to burning velocity, the closer the stagnation plane moves toward the flame front, and the greater is the flow gradient that stretches each new element of flame surface. One can readily obtain an analytical solution to the problem of determining the position of the stagnation point. Combining equation 17 and equation 20 for the flow velocity at the top of the sphere, where  $\theta = 0$ , and using the near-limit value for the expansion ratio  $\rho_u/\rho_b = 5$ , one obtains

$$v_{net} = v_r(\text{combustion}) + v_r(\text{buoyancy}) = 4S_u \left(\frac{r_0}{r}\right)^2 - v_b + \frac{3}{2} v_b \frac{r_0}{r} - \frac{1}{2} v_b \left(\frac{r_0}{r}\right)^3. \quad (21)$$

Setting  $\eta = v_b/S_u$  and setting  $v_{net} = 0$  at the stagnation point gives the following cubic equation:

$$\left(\frac{r_s}{r_0}\right)^3 - \frac{3}{2} \left(\frac{r_s}{r_0}\right)^2 - \frac{4}{\eta} \left(\frac{r_s}{r_0}\right) + \frac{1}{2} = 0. \quad (22)$$

The position of that stagnation point at  $\theta = 0$  is plotted in figure 15 as a function of  $\eta$ , the ratio of buoyant velocity to burning velocity. Clearly, as the burning velocity diminishes and/or the buoyant velocity increases, the stagnation point moves closer to the flame front. The closer it moves to the the flame front the greater is the stretch velocity gradient. Extinction occurs at a finite value of that gradient and the previous arguments suggest that the finite value of the gradient corresponds to a minimum burning velocity of about 3 cm/sec for "normal" flames. Such "normal" flames are flames that are burning in earth's gravity and are driven by exothermic reactions that are essentially irreversible so that the expansion ratio  $\rho_u/\rho_b$  is reasonably large and the buoyancy force is finite.

There are several complications that have not been considered that would influence this analysis. First is the fact that the flow solutions depicted in figures 13, 14, and 15 are quasi-steady-state approximations. In reality, the correct solutions should be time-dependent ones for the dynamic processes. The quasi-steady-state approximations were obtained by the superposition of two steady-state solutions for fully developed flow conditions. The time-dependent, dynamic details of the developing flows can differ in some respects from these quasi-steady-state solutions. In addition, the real flows in the presence of both forces acting simultaneously are not simply equal to the vector sum of the flows generated by each force acting independently. Secondly, the buoyancy-induced flows develop dynamically and cannot, as has been assumed, instantaneously follow the solutions represented by equations 17 and 18. Inertial forces prevent an instantaneous response to increasing fireball size,

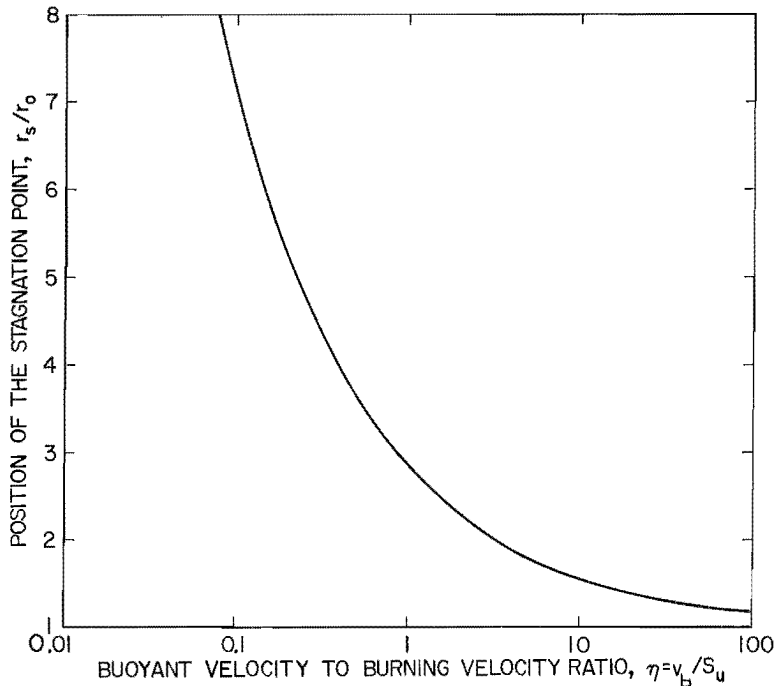


FIGURE 15. - Position of the stagnation point above the upward hemisphere of a rising and expanding flame kernel as a function of the ratio of buoyant velocity to burning velocity.

and additional flows provide a drag force limitation on  $v_b$ .

To illustrate this second complication, consider substituting equation 11 into the expression for  $\eta$ . For air expansion ratio of  $\rho_u/\rho_b = 5$  and  $g = 980 \text{ cm/sec}^2$  one obtains

$$\begin{aligned} \eta &= v_b/S_u = \frac{4}{105} \frac{gr}{S_u^2} \\ &= 37.38 \frac{r(\text{cm})}{S_u^2(\text{cm sec}^{-1})}. \end{aligned} \quad (23)$$

This gives an  $\eta$ -value which increases linearly with  $r$  regardless of the initial value of  $S_u$ . For example for a near stoichiometric methane-air mixture with  $S_u = 44 \text{ cm/sec}$  one would obtain an  $\eta$ -value of 10 for a spherical fireball of about 5 m in radius. An  $\eta$ -value of 10 exceeds the normal upward quenching limit so that there is an implication from the equations that even upward propagation will

always eventually quench for a large enough fireball. In reality, inertial forces prevent such an instantaneous response to increasing fireball size.

In any case, it is somewhat of a moot point, however, for an object above such a fireball as to whether it is overtaken by a "propagating" flame front or whether buoyancy convects that same flame front to it. In either case, the object is overtaken by the front.

The final complexity that requires consideration is the choice of a proper  $S_u$ -value during the time that the flame stretch process is exerting its influence. As indicated earlier, in the presence of flame stretch the burning velocity must decrease to less than its laminar, adiabatic or ideal value. On the basis of previous considerations, to a first approximation, in the presence of a velocity gradient, one obtains:  $S_u = (S_u)_{\text{ideal}} - (S_u)_e$ . Thus the presence of stretch reduces  $S_u$ , which increases  $\eta$ , which further reduces  $S_u$ , which further increases  $\eta$ . It is this feedback interaction that is probably responsible for the actual extinction process for upward propagation. The available data suggests that the feedback process is not significant for  $\eta < \rho_u/\rho_b$ . As has been argued in a previous publication (2), the condition  $\eta = v_b/S_u = \rho_u/\rho_b$  corresponds to the downward propagation limit. At some point for  $\eta > \rho_u/\rho_b$ , the above feedback process becomes increasingly significant and soon leads to extinction of the upward propagating hemisphere as well.

A more exact consideration of this problem awaits a more exact solution to the time-dependent Navier-Stokes equations for the system considered under a set of constraints that reflect the realistic feedback process by which stretch gradients reduce the actual burning velocity of the stretched flame.

## REFERENCES

1. Hertzberg, M. The Theory of Flammability Limits. Natural Convection. BuMines RI 8127, 1976, 15 pp.
2. \_\_\_\_\_. The Theory of Flammability Limits. Conductive-Convective Wall Losses and Thermal Quenching. BuMines RI 8469, 1980, 25 pp.
3. \_\_\_\_\_. The Theory of Flammability Limits. Radiative Losses and Selective Diffusional Demixing. BuMines RI 8607, 1982, 38 pp.
4. Warnatz, J. The Structure of Laminar Alkane-, Alkene- and Acetylene-Flames. Paper in Eighteenth Symposium (International) on Combustion (Waterloo, Ontario, Canada, Aug. 17-22, 1980). Combustion Inst., Pittsburgh, PA, 1981, pp. 369-384.
5. Karlovitz, B., D. W. Denniston, Jr., D. H. Knapschaefer, and F. E. Wells. Studies on Turbulent Flames. Paper in Fourth Symposium (International) on Combustion (Cambridge, Mass., Sept. 1-5, 1952). Williams and Wilkins Co., Baltimore, MD, 1953, pp. 613-620.
6. Lewis, B., and G. von Elbe. Combustion, Flames and Explosions of Gases. Academic, 2d ed., 1961, 731 pp.
7. Markstein, G. H. Non-Steady Flame Propagation. Macmillan, 1964, 328 pp.
8. Mache, H., and A. Hebra. Measurement of the Burning Velocity of Explosive Gas Mixtures. Sitzber. Akad. Wiss. Wien, v. 150, 1941, p. 157.
9. Gunter, R., and A. Janisch. Measurements of Burning Velocity in a Flat Flame Front. Combust. and Flame, v. 19, 1972, p. 49.
10. Grumer, J., M. E. Harris, and H. Schultz. Flame Stabilization on Burners With Short Ports or Non Circular Ports. Paper in Fourth Symposium (International) on Combustion (Cambridge, Mass., Sept. 1-5, 1952). Williams and Wilkins Co., Baltimore, MD, 1953, pp. 695-701.
11. Grumer, J., M. E. Harris, and V. R. Rowe. Fundamental Flashback, Blowoff, and Yellow-Tip Limits of Fuel Gas-Air Mixtures. BuMines RI 5225, 1956, 199 pp.
12. Hertzberg, M. The Flammability Limits of Gases, Vapors and Dusts: Theory and Experiment. Paper in Proceedings of the International Conference Meeting on Fuel-Air Explosions (McGill Univ., Montreal, Canada, Nov. 4-6, 1981). Univ. Waterloo Press, Study No. 16, Waterloo, Canada, 1982, pp. 3-48.
13. Hertzberg, M., K. L. Cashdollar, C. D. Litton, and D. Burgess. The Diffusion Flame in Free Convection. Buoyancy-Induced Flows, Oscillations, Radiative Balance, and Large-Scale Limiting Rates. BuMines RI 8263, 1978, 33 pp.
14. Reed, S. B., P. Datta, and J. Mineur. The Effect of Vitiating of Combustion Air on Laminar Flame Stability. J. Inst. Fuel, v. 111, 1971, p. 111.
15. Edmondson, H., and M. P. Heap. A Precise Test of the Flame-Stretch Theory of Blow-off. Paper in Twelfth Symposium (International) on Combustion (Poitiers, France, July 14-20, 1968). Combustion Inst., Pittsburgh, PA, 1969, pp. 1007-1014.

16. Edmondson, H., and M. P. Heap. Blowoff of Inverted Flames. *Combust. and Flame*, v. 14, 1970, p. 191.
17. Kawamura, T., K. Asato, T. Mazaki, T. Hamaguchi, and H. Kayahara. Explanation of the Blowoff of Inverted Flames by the Area-Increase Concept. *Combust. and Flame*, v. 35, 1979, pp. 109-116.
18. Melvin, A., and J. B. Moss. Evidence for the Failure of the Flame Stretch Concept for Premixed Flames. *Combust. Sci. and Technol.*, v. 7, 1973, p. 189.
19. Potter, A. E., S. Heimel, and J. H. Butler. Apparent Flame Strength. A Measure of Maximum Reaction Rate in Diffusion Flames. Paper in Eighth Symposium (International) on Combustion (Pasadena, Calif., Aug. 28 - Sept. 3, 1960). Williams and Wilkins Co., Baltimore, MD, 1962, pp. 1027-1034.
20. Pandya, T. P., and F. J. Weinberg. The Study of the Structure of Laminar Diffusion Flames by Optical Methods. Paper in Ninth Symposium (International) on Combustion (Ithaca, N.Y., Aug. 27-Sept. 1, 1962). Academic, 1963, pp. 587-596.
21. Yamaoko, I., and H. Tsuji. An Experimental Study of Flammability Limits Using Counterflow Flames. Paper in Seventeenth Symposium (International) on Combustion (Leeds, England, Aug. 20-25, 1978). Combustion Inst., Pittsburgh, PA, 1979, pp. 843-855.
22. Law, C. K., S. Ishizuka, and M. Mizomoto. Lean Limit Extinction of Propane/Air Mixtures in the Stagnation-Point Flow. Paper in Eighteenth Symposium (International) on Combustion (Waterloo, Ontario, Canada, Aug. 17-22, 1980). Combustion Inst., Pittsburgh, PA, 1981, pp. 1791-1798.
23. Ishizuka, S., K. Miyasaka, and C. K. Law. Effects of Heat Loss, Preferential Diffusion, and Flame Stretch on Flame-Front Instability and Extinction of Propane/Air Mixtures. *Combust. and Flame*, v. 45, 1982, p. 293.
24. Ishizuka, S., and C. K. Law. An Experimental Study on Extinction and Stability of Stretched Premixed Flames. Paper in Nineteenth Symposium (International) on Combustion (Haifa, Israel, Aug. 8-13, 1982). Combustion Inst., Pittsburgh, PA, 1983, p. 327.
25. Hertzberg, M. Discussion. Fourteenth Symposium (International) on Combustion (University Park, Pa., Aug. 20-25, 1972). Combustion Inst., Pittsburgh, PA, 1972, pp. 1127-1128.
26. Coward, H. F., and G. W. Jones. Limits of Flammability of Gases and Vapors. *BuMines B 503*, 1952, 155 pp.
27. Zabetakis, M. G. Flammability Characteristics of Combustible Gases and Vapors. *BuMines B 627*, 1965, 121 pp.
28. Egerton, A. C. Limits of Inflammability. Paper in Fourth Symposium (International) on Combustion (Cambridge, MA, Sept. 1-5, 1952). Williams and Wilkins Co., Baltimore, MD, 1953, p. 4.
29. Linnett, J. W., and C. J. S. M. Simpson. Limits of Inflammability. Paper in Sixth Symposium (International) on Combustion (New Haven, Conn., Aug. 19-24, 1956). Reinhold, 1956, p. 20.

30. Levy, A. An Optical Study of Flammability Limits. Proc. Roy. Soc. (London), Ser. A, v. 283, 1965, p. 134.
31. Dixon-Lewis, G. Discussion. Sixth Symposium (International) on Combustion (New Haven, Conn., Aug. 19-24, 1956). Reinhold, 1956, p. 26.
32. Dixon-Lewis, G., and G. L. Isles. Limits of Flammability. Paper in Seventh Symposium (International) on Combustion (London and Oxford, England, Aug. 28-Sept. 3, 1958). Butterworth, 1959, p. 475.
33. Altenkirch, R. A., Eickhorn, N. N. Hsu, A. B. Brancic, and N. E. Cevallos. Characteristics of Laminar Gas Jet Diffusion Flames Under the Influence of Elevated Gravity. Paper in Sixteenth Symposium (International) on Combustion (Cambridge, Mass., Aug. 15-21, 1976). Combustion Inst., Pittsburgh, PA, 1977, pp. 1165-1174.
34. von Lavante, E., and R. A. Strehlow. The Mechanism of Lean Limit Flame Extinction. Combust. and Flame, v. 49, 1983, pp. 123-140.
35. Landau, L. D., and E. M. Lifshitz. Fluid Mechanics. Addison-Wesley, 1959, pp. 63-68.

## APPENDIX.--SYMBOLS AND NOMENCLATURE

$\alpha$	The spatially average or effective diffusivity of the flame zone gases.
$A_s$	The surface area of the flame front.
$c$	The spatially averaged heat capacity of the flame zone, or a mixing zone.
$\delta$	The flame zone or flame front thickness.
$\Delta x$	The flame zone thickness.
$d_q$	The tubular wall-loss quenching diameter.
$\Delta v$	The change in unburned gas velocity across the flame zone thickness.
$\frac{dp}{dz}$	The axial pressure gradient along a tube.
$\frac{dv}{dx}$	The velocity gradient stretching a propagating flame front.
$\eta$	The ratio of buoyant velocity to burning velocity; also the gas viscosity.
$g$	The gravitational acceleration.
$g_0$	The value of $g$ at the surface of the earth.
$g_b$	The boundary velocity gradient.
$k$	A constant of proportionality.
$K$	The Karlovitz number.
$\ell$	The distance between a nozzle exit plane and a stagnation plate, or the distance between counterflowing nozzles.
$L$	A characteristic length proportional to the flame zone thickness.
$Pe$	The Peclet number for tubular wall-loss quenching.
$\dot{q}$	The volumetric flame front heating (or cooling) rate.
$\rho$	The mass density of a gas.
$\rho_u, \rho_b$	The density of the unburned and burned gases, respectively.
$r$	A radial coordinate; the radius of an expanding flame kernel or of a fireball; the radius of curvature of a flame front; the radial distance from the axis of a tube or from the center of a fireball.
$r_0$	The radius of a tube; the radius of a sphere.
$S_u$	The burning velocity; the velocity of a flame front relative to the unburned gas.
$(S_u)_a$	The horizontal limit burning velocity for quenching by natural convection.

$(S_u)_{a\downarrow}$	The downward stagnation limit burning velocity.
$(S_u)_{a, e\uparrow}$	The upward limit burning velocity for quenching by flame stretch (process e) induced by buoyancy (process a).
$(S_u)_b$	The limit burning velocity for conductive-convective wall-loss quenching.
$(S_u)_c$	The limit burning velocity for radiative loss quenching.
$(S_u)_e$	The limit burning velocity for quenching by flow gradient effects or flame stretch.
$(S_u)_{ideal}$	The true or ideal laminar burning velocity.
$S_b$	The outward speed of a spherical flame front with respect to the laboratory observer.
$\theta$	The polar coordinate.
$\tau_{pm}$	The characteristic time for the completion of the combustion reactions within a propagating flame front.
$\tau_r$	The characteristic residence time for reactants flowing near and into a propagating flame front.
$t$	The time.
$T$	The temperature.
$T_b$	The temperature of burned gases.
$T_u$	The temperature of unburned gases.
$v$	A velocity.
$v_n$	The cold gas velocity component normal to the flame front.
$v_b(t)$	The buoyant rise velocity of the center of mass of a spherically expanding fireball.
$v_r$	The radial velocity component of the buoyancy-induced unburned gas flow past a sphere or spherical fireball.
$v_\theta$	The tangential or polar velocity component of the buoyancy-induced unburned gas flow past a sphere or spherical fireball.
$v_r(r)$	The outward radial velocity of expansion for the unburned gas that is induced by the combustion force in spherical propagation.
$v_{net}$	The net radial flow velocity at $\theta = 0$ , above a spherically propagating combustion wave.
$V_\delta$	The flame front volume.
$x$	The propagation direction.